How does the shape of the wing and hindlimb bones of aquatic birds relate to their locomotor abilities?

Martin Segesdi, Delphine Brabant, Raphaël Cornette, Alexandra Houssaye

Received: 20 November 2023 | Revised: 7 May 2024 | Accepted: 8 May 2024

DOI: 10.1002/ar.25512

RESEARCH ARTICLE

The Anatomical Record WILEY

How does the shape of the wing and hindlimb bones of aquatic birds relate to their locomotor abilities?

Martin Segesdi[1,2,3] | **Delphine Brabant**[4] | **Raphaël Cornette**[5] | **Alexandra Houssaye**[6]

[1]Department of Paleontology, ELTE Eötvös Loránd University, Institute of Geography and Earth Sciences, Budapest, Hungary

[2]Department of Zoology, Hungarian Natural History Museum, Budapest, Hungary

[3]Department of Paleontology and Geology, Hungarian Natural History Museum, Budapest, Hungary

[4]Plateforme Surfaçus, Délégation de l'Innovation Numérique, Direction générale déléguée aux collections, Muséum National d'Histoire Naturelle, Paris, France

[5]Institut de Systématique, Evolution, Biodiversité (ISYEB), Muséum National d'Histoire Naturelle, CNRS, Sorbonne Université, EPHE, Université des Antilles, Paris, France

[6]Mécanismes adaptatifs et évolution (MECADEV), UMR 7179, MNHN, Paris, France

Correspondence
Martin Segesdi, Department of Paleontology, ELTE Eötvös Loránd University, Institute of Geography and Earth Sciences, 1117, Pázmány Péter sétány 1/c, Budapest, Hungary.
Email: blackadder42@student.elte.hu

Funding information
Erasmus+ programme and Tempus Public Foundation, Grant/Award Numbers: CM-SMP-KA103/295472/2018, 2021-1-HU01-KA131-HED-000003804

Abstract

Aquatic birds represent diverse ecologies and locomotion types. Some became flightless or lost the ability for effective terrestrial locomotion, yet, certain species excel in water, on land, and in air, despite differing physical characteristics associated with each medium. In this exploratory study, we intend to quantitatively analyze the morphological variety of multiple limb bones of aquatic birds using 3D geometric morphometrics. Morphological variation is mainly driven by phylogeny, which also affects size and locomotion. However, the shape of the ulna, including the proportion and orientation of the epiphyses is influenced by size and aquatic propulsive techniques even when phylogeny is taken into consideration. Certain trends, possibly linked to functions, can be observed too in other bones, notably in cases where phylogenetic and functional signals are probably mixed when some taxa only englobe species with similar functional requirements: penguins exhibit the most distinctive wing bone morphologies, highly adapted to wing-propulsion; advanced foot-propellers exhibit femur morphology that reduces proximal mobility but supports stability; knee structures, like cnemial crests of varied sizes and orientations, are crucial for muscle attachments and efficient movement in water and on land; taxa relying on their feet in water but retaining terrestrial abilities share features enabling swimming and walking postures. Size-linked changes distinguish the wing bones of non-wing-propelled taxa. For hindlimbs, larger size relates to robust bones probably linked to terrestrial abilities, but robustness in femora can be connected to foot-propulsion. These results help us better understand birds' skeletal adaptation and can be useful inferring extinct species' ecology.

KEYWORDS

3D geometric morphometrics, aquatic adaptation, aquatic birds, functional morphology, limb bone anatomy

1 | INTRODUCTION

During the evolutionary history of tetrapods, several lineages adapted secondarily to an aquatic lifestyle (Kelley & Pyenson, 2015; Motani & Vermeij, 2021). Since water and air present highly different physical characteristics (Gutarra & Rahman, 2022), animals that usually move in both media have to face distinct mechanical constraints using the same musculoskeletal system. Although on land bodies are mostly affected by gravity, in the water column this constraint is counterbalanced by buoyancy; however, drag forces, acting opposite to the motion, are stronger than in air (Hustler, 1992; Kooyman, 1989; Lovvorn et al., 2001). The adaptation of various secondarily aquatic clades to face these challenges required specific solutions and has resulted, in many cases, in convergent forms (Houssaye, 2009; Houssaye & Fish, 2016; Motani & Vermeij, 2021; Smith et al., 2021; Watanabe et al., 2021).

Birds illustrate aquatic behaviors on a wide range, from shorebirds to persistent surface paddlers and skilled divers (Ashmole, 1971), and are one of the most significant tetrapod groups of both marine and freshwater ecosystems (Ainley, 1980; Shealer, 2002). In water, propulsion can be provided by the forelimbs (wing-propulsion) and/or the hindlimbs (foot-propulsion) (Ashmole, 1971; Fish, 2016; Segesdi & Pecsics, 2022; Storer, 1945; Townsend, 1909). But beyond aquatic locomotion, several aquatic species have retained both terrestrial and aerial skills to some extent, and are able to dive, fly, and walk on a substrate effectively (Provini et al., 2012a; Storer, 1945). Conversely, the more derived wing-propellers (e.g., penguins) became flightless (Louw, 1992; Watanabe et al., 2021), while the most capable foot-propelled taxa (e.g., grebes, loons) have lost much of their terrestrial abilities (Clifton et al., 2018). The locomotor abilities and behavior of certain species remain nevertheless difficult to understand because of the small number of available observations in nature (discussed in Lapsansky & Armstrong, 2022). Birds best adapted to diving have usually smaller wings (high wing-loading) than non-divers, regardless of whether they prefer wing- or foot-propulsion (Lapsansky et al., 2022). In addition, wing-propelled birds have more robust wing bones with a generally flattened diaphysis (Serrano et al., 2020; Smith et al., 2021). Nevertheless, joint mobility does not decrease in volant wing-propelled taxa (Raikow et al., 1988), although flightless penguins are characterized by almost rigid distal joints in their wings (Louw, 1992; Schreiweis, 1982). In foot-propelled species, the mobility of the hip and knee joints might be reduced to varying degrees, especially in taxa (e.g., grebes and loons) in which the femur and the proximal tibiotarsus are situated alongside the ribcage and are enclosed within the skin covering the abdomen, to increase the streamlining of the body (Clifton et al., 2018). Moreover, the morphology of the knee joint is closely related to swimming and diving efficiency, with markedly elongated cnemial crests at the proximal end of the tibiotarsus or large patellae providing attachment sites for powerful muscles enhancing foot-propulsion (Clifton et al., 2018).

This study aims to quantitatively analyze the morphological variety of limb long bones of birds with diverse aquatic habits, using a 3D geometric morphometric approach. We intend to see if morphology could distinguish different terrestrial, aquatic, or aerial locomotion habits. Although 3D geometric morphometric methods were already used to study bird bones, our paper is the first attempt to focus on multiple limb elements from both the wing and the hindlimb in aquatic taxa. Three-dimensional methods, by taking into consideration the whole bone shape, are useful tools to describe phenotypic variations beyond two-dimensional ratios, to gain a better understanding of the complexity of shape changes (Adams, 2014; Bjarnason & Benson, 2021; Bookstein, 1991; Navalón et al., 2022). Moreover, they also enable us to quantitatively assess the effect of allometry and of the phylogenetic heritage on the bones' shape. We expect that while the morphology of wing bones will be most of all connected to aerial or wing-assisted aquatic movements, hindlimb bones will show more complex signals reflecting rather efficiency in body weight support, foot-assisted aquatic movements, and/or even manipulative skills. We hypothesize that the most differing locomotor habits will be associated with highly different morphologies for the bones or body regions involved. We assume that the morphological disparity of the bones will reflect that some highly specific aquatic locomotor habits may influence or even eclipse other locomotor abilities. We also expect that flightless taxa, especially penguins, will show major morphological differentiation from other birds, due to both their large body size and specific locomotor behaviors.

2 | MATERIALS AND METHODS

2.1 | Sampling and data acquisition

Thirty-one dry skeletons from 18 extant bird species were sampled (Table 1). They belong to six avian families (Anatidae, Podicipedidae, Alcidae, Phalacrocoracidae, Procellariidae, Spheniscidae) (Table 1, Figure 1), and at least two specimens were sampled from every studied family. There is a large number of known birds with swimming and diving habits. Although limited in size, our sample illustrates various locomotor abilities, body masses, and aquatic ecologies representative of different branches of the bird's phylogeny (see Table 2). The material is housed in the collections of the

TABLE 1 List of the studied specimens and sampled bones (see Supplementary I for common names, body mass and locomotion mode of the studied species).

	No.	Species	Specimen number	H	R	U	F	T
Anatidae	1	*Tachyeres pteneres*	MNHN-ZO-AC-1990-24	X	X	X	X	X
	2	*Tachyeres pteneres*	MNHN-ZO-AC-1993-69		X	X	X	X
	3	*Anas penelope*	MNHN-ZO-AC-1996–70	X	X	X	X	X
	4	*Anas penelope*	MNHN-ZO-AC-1992-22	X	X	X	X	X
	5	*Mergus merganser*	MNHN-ZO-AC-2004-192	X	X	X	X	X
	6	*Mergus merganser*	MNHN-ZO-AC-IV-1177	X	X	X	X	X
Podicipedidae	7	*Podiceps cristatus*	MNHN-ZO-AC-1933-7	X	X	X	X	X
	8	*Podiceps cristatus*	MNHN-ZO-AC-1997-966	X	X	X	X	X
Alcidae	9	*Fratercula arctica*	MNHN-ZO-AC-1997-359	X	X	X		
	10	*Fratercula arctica*	MNHN-ZO-AC-1997-360	X	X	X	X	X
	11	*Uria aalge*	MNHN-ZO-AC-1997-364	X	X	X	X	X
	12	*Uria aalge*	MNHN-ZO-AC-1997-369	X	X	X	X	X
	13	*Alca torda*	MNHN-ZO-AC-1997-355	X	X	X		X
	14	*Alca torda*	MNHN-ZO-AC-1997-681	X	X	X	X	X
	15	*Alle alle*	MNHN-ZO-AC-1997-682	X	X	X	X	X
	16	*Alle alle*	MNHN-ZO-AC-1997-357	X	X	X	X	X
Phalacrocoracidae	17	*Phalacrocorax carbo*	MNHN-ZO-AC-2004-193	X	X	X	X	X
	18	*Phalacrocorax carbo*	MNHN-ZO-AC-1999-142	X	X	X	X	X
Procellariidae	19	*Pelecanoides georgicus*	MNHN-ZO-AC-2010-235	X	X	X	X	X
	20	*Pelecanoides urinatrix*	MNHN-ZO-AC-1997-127	X	X	X	X	X
Spheniscidae	21	*Aptenodytes patagonicus*	MNHN-ZO-AC-1997-111	X	X	X	X	X
	22	*Aptenodytes patagonicus*	MNHN-ZO-AC-2004-380	X	X	X	X	X
	23	*Aptenodytes patagonicus*	MNHN-ZO-AC-2004-381	X	X	X	X	X
	24	*Aptenodytes patagonicus*	MNHN-ZO-AC-2004-382	X	X	X	X	X
	25	*Pygoscelis adeliae*	MNHN-ZO-AC-1997-101	X	X	X	X	X
	26	*Pygoscelis papua*	MNHN-ZO-AC-1993-90	X	X	X	X	X
	27	*Spheniscus humboldti*	MNHN-ZO-AC-1997-114	X	X	X	X	
	28	*Spheniscus humboldti*	MNHN-ZO-AC-1997-744	X	X	X	X	X
	29	*Spheniscus demersus*	MNHN-ZO-AC-1997-100	X	X	X	X	X
	30	*Eudyptes chrysocome*	MNHN-ZO-AC-1997-112	X	X	X	X	X
	31	*Eudyptes chrysolophus*	MNHN-ZO-AC-1914-191	X	X	X	X	X

Abbreviations: F, femur; H, humerus; R, radius; T, tibiotarsus; U, ulna.

Muséum National d'Histoire Naturelle, Paris, France (MNHN). We followed the taxonomic determination given by the institution. Our study focuses on the most proximal long bones, assuming they are more involved in propulsion, although other limb elements can naturally also show a strong functional signal, like the tarsometatarsus (De Mendoza & Gómez, 2022). We therefore sampled stylopod (humerus and femur), and zeugopod (ulna and radius) elements, and we also took into account the partial zeugopod-partial autopod tibiotarsus. Bones with fractures or signs of pathologies on their surface were excluded from the analysis, as well as fibulae, since in many cases they were missing, damaged, or not attached to their original anatomical position. We sampled only adult specimens based on macroscopic morphological features and the ossification of the epiphyses (Watanabe, 2018). Our sample is thus made of 150 bones: 30 humeri, 31 radii, 31 ulnae, 29 femora, and 29 tibiotarsi. Information regarding the sex of the sampled specimens was not available (see Supplementary I). Bones from the left side of the body were arbitrarily chosen; when left bones were not available, the right ones were digitally

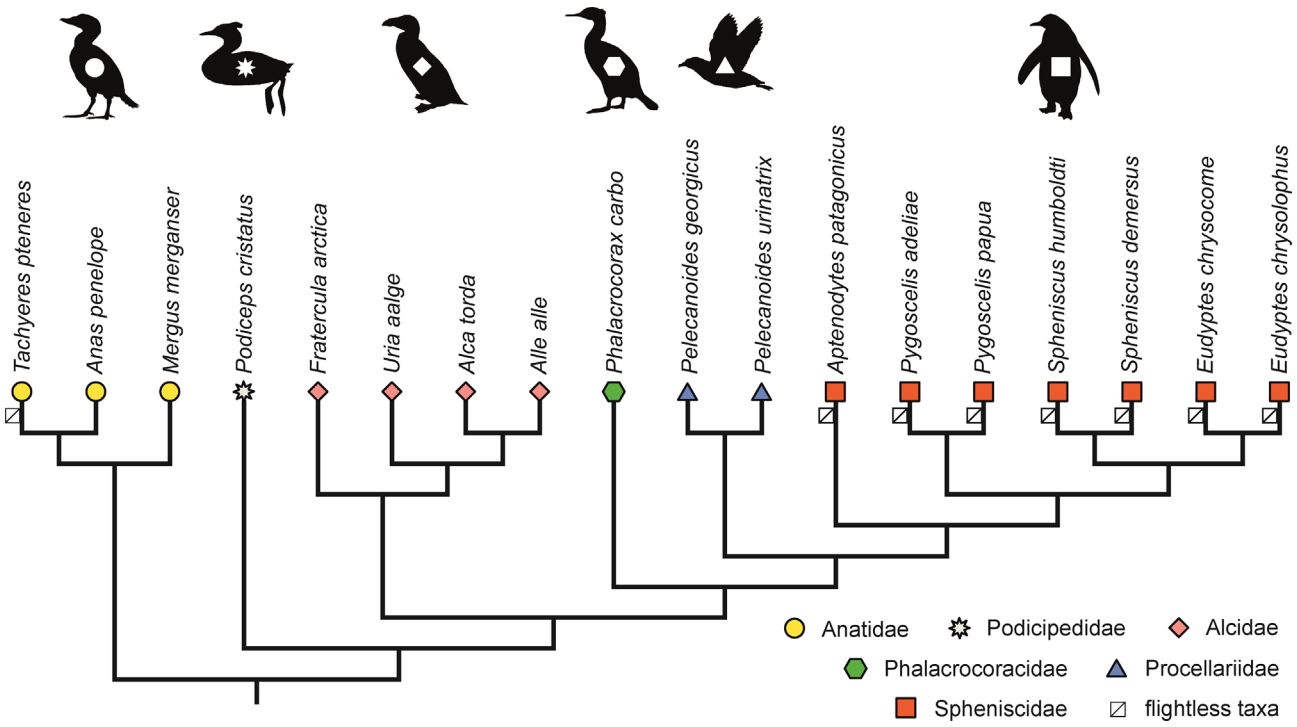

FIGURE 1 Composite phylogenetic tree of the studied species following Jarvis et al. (2014) for the high systematic level, Gonzalez et al. (2009) for Anatidae, Moum et al. (2002) for Alcidae, and Bertelli and Giannini (2005) for Spheniscidae. The position of *Fratercula arctica* within Alcidae is based on Friesen et al. (1996). Silhouettes were downloaded from PhyloPic (http://phylopic.org/). End node symbols and colors are identical to the symbols of principal component analyses and neighbor joining trees.

	FP ✓	FP ⃠	WP ✓	WP ⃠	Volant	Flightless	Clumsy	Mobile
A. penelope	X			X	X			X
T. pteneres	X		X (?)			X		X
M. merganser	X		X		X			X
P. cristatus	X			X	X		X	
P. carbo	X			X	X			X (?)
F. arctica		X	X		X			X
U. aalge		X	X		X		X	
A. torda		X	X		X		X	
A. alle		X	X		X		X	
P. georgicus		X	X		X		X	
P. urinatrix		X	X		X		X	
A. patagonicus		X	X			X		X
P. adeliae		X	X			X		X
P. papua		X	X			X		X
S. humboldti		X	X			X		X
S. demersus		X	X			X		X
E. chrysocome		X	X			X		X
E. chrysolophus		X	X			X		X

Abbreviations: FP, foot-propulsion; WP, wing-propulsion.

TABLE 2 List of the studied species with their locomotor performances. All studied species were categorized depending on what was reported in the literature: to use (✓), or not to use (⃠) their foot and/or wings for propulsion in water. Birds are also grouped based on their aerial (volant or flightless) and terrestrial skills (clumsy or mobile). References for each species are provided in Supplementary I.

mirrored for the analysis using MeshLab software (Cignoni et al., 2008). A blue light fringe Breuckmann 3D (SmartSCAN-3D) surface scanner (0.001 mm resolution) and a FAROArm Edge scanner with FAROBluTM laser (0.05 mm resolution) were used for bone digitization in three dimensions, depending on specimen size.

2.2 | Anatomical terminology

For the osteological descriptions, we followed the nomenclature of Baumel et al. (1993), completed by Watanabe et al. (2021). Myological nomenclature follows Watanabe et al. (2021) for the wing bones and Clifton et al. (2018) for the hindlimbs'. Topographic terms of orientation used herein to describe landmarks' position follow those adopted by Clark (1993), and are based on the following posture: the bird stands upright on its two hindlimbs with the femorotibial joints slightly flexed, while the wings—or flippers in the case of penguins (Spheniscidae)—are outstretched and held away from the body laterally. To determine the orientation of the unique forelimbs of the penguin specimens, we followed Schreiweis (1982), Louw (1992), and Watanabe et al. (2021).

2.3 | Landmark digitization

The bones' shape was defined with anatomical landmarks, which were placed manually on homologous locations using the IDAV Landmark Editor software package (Wiley et al., 2005). These landmarks belong to type I and type II of Bookstein (1991) as they represent intersections of tissues and minima/maxima of curvatures, respectively. We used 20 landmarks on the humerus, 11 on the radius, 9 on the ulna, 27 on the femur, and 25 on the tibiotarsus. Description and position of landmarks for each bone are provided in Supplementary II where points are shown on the bones of arbitrarily chosen taxa (Figures S7–S11). Furthermore, because the morphology of wing bones was extremely varying, the position of landmarks is shown on a spheniscid and on another specimen from a different family.

2.4 | Visualization of repeatability

Repeatability of the pose of the landmarks was verified and visualized based on measurements taken 10 times on each bone of three *Aptenodytes patagonicus* specimens (MNHN-ZO-AC-1997-111, MNHN-ZO-AC-2004-380, MNHN-ZO-AC-2004-381) since this species was represented with the highest number of specimens in our dataset. The measurements were superimposed with GPA; then the results were visualized using PCAs. The variability of the measurements for each specimen was clearly smaller than the inter-individual variability so that our landmark set appeared appropriate enough to carefully describe the morphological variation within our dataset (see Supplementary IV: Figure S12 for PCAs).

2.5 | Geometric morphometrics

Measurements were superimposed applying generalized procrustes analysis (GPA) (Gower, 1975; Rohlf & Slice, 1990), with the usage of the "geomorph" package in R environment (R Development Core Team, 2014) (see Supplementary III for code used for the analysis). GPA translates, scales, and rotates the landmark sets, to remove the effects of size, angle, and of the relative position of specimens in the coordinate system. This analysis serves to minimize the sum of square distances between landmark configurations and to isolate only the information of shape (Bookstein, 1991). We performed Neighbor Joining trees (NJT) (using "ape" package in R), to make a global visualization (on the whole variance) of the phenotypic variability between the studied specimens (Paradis et al., 2004) (see Supplementary V). Trees were computed based on the relative Euclidian distances between specimens, derived from principal component scores (Baylac & Frieß, 2005). Then we used principal component analyses (PCA) to explore shape variation (Baylac & Frieß, 2005; Gunz & Mitteroecker, 2013). We focused our discussion on those PCA axes that are most of all relevant to our questions, that is, that separate different groups (including different locomotor habits), and are not related to intraspecific variability. Since the wing bones of penguins are markedly distinct from those of the other families in our sample, this separation consists of most of the variation occurring on PC1. We thus ran additional analyses after excluding this family, for the humerus, radius, and ulna.

To illustrate theoretical extreme shapes along the PCA axes, TPS (Thin-Plate Spline) deformation was applied (using "morpho" package in R). TPS is a useful interpolation tool to flexibly warp 3D surfaces depending on the reference landmark configuration (Bookstein, 1991; Gunz et al., 2009; Mitteroecker & Gunz, 2009). To perform this, first, we chose a specimen closest to the average (based on principal component scores); then the average landmark configuration was calculated and, based on this, the model of the average specimen was warped into a mean shape. Hereafter this mean shape was warped into the theoretical extremes of the given axis. When describing theoretical shapes, we focused on the regions covered by landmarks, because although TPS based on anatomical landmarks helps to visualize global shape changes, curvatures are not necessarily

relevant on areas without landmark coverage due to the higher degree of interpolation.

2.6 | Tests of the link between bone shape and locomotion

In Table 2, we summarized if the given species was reported in the literature to use (or not to use) its foot and/or wings for primary propulsion in water. The focus of the categorization was on propulsive use only. If precise observations regarding the given species were not available, we relied on the data related to the given genus or family (see Supplementary I for details and references about the locomotion groups). We also categorized the species in relation to their aerial and terrestrial abilities. By flightless we refer to species that are unable neither to glide nor to perform a powered flight; otherwise, they are marked as volant. By clumsy we mark species that have limited terrestrial abilities; in the opposite case, they are mentioned as mobile (see Supplementary I). To evaluate to what extent the phenotypic similarities follow the presence or absence of foot- (FP) and wing-propulsion (WP), the aerial and the terrestrial skills, we used a *k*-Nearest-Neighbor (*k*-NN) algorithm (using "class" package in R) (Ripley, 2007; Venables & Ripley, 2002). This algorithm categorizes an object into a predefined group based on its Euclidian distance with its *k*-Nearest-Neighbor (where k is a natural number) and has the advantage of being usable for small samples. We tested with k ranging from 1 to $n - 1$ (where n is the lowest number of individuals in the group for the given analysis); then the mean of the obtained results was computed (following Bader et al., 2022). Thus 4 *k*-NN predictions were performed for each bone: absence versus presence of FP, absence versus presence of WP, clumsy versus mobile, and flightless versus volant. The *k*-NN predictions indicate the probability of a specimen to be correctly placed in the above defined categories based on the shape of the given bone. To ensure testing consistency, all categories were examined across all bones, although the link between locomotor categories and morphology was not necessarily obvious in the case of bones from limbs not directly involved in the type of movement (e.g., the relationship between terrestrial abilities and wing bone morphology). We also computed the likelihood of random correct classification, especially given our small sample size, based on the percentage of individuals in the largest of the two groups. The level at which the effectiveness of *k*-NN prediction, when relying on morphology, surpasses the probability of random classification is represented by the baselines on the associated figure.

2.7 | Tests of allometry effect and phylogenetic signal

To assess the effect of allometry—size-linked changes of morphological traits (Klingenberg, 2016)—we performed a Pearson's product moment correlation test, to evaluate the correlation between the centroid sizes ($\log_{10}$ transformed) and the principal components for each bone studied, per axis (Table 3). Centroid size (Cs) is determined as the square root of the sum of squared distances of every landmarks of an object from their center of gravity (centroid) (Klingenberg, 2016). We also projected (on PC axes) each species' average body mass, based on Dunning (2008) to illustrate its relationship with shape (see Supplementary I: Figure S1). To understand the influence of allometry on bone morphology, we tested the covariation between whole shape and centroid size with Procrustes analyses of variance using the *procD.lm* function ("geomorph" package); when significant association was found, theoretical shapes at the Cs minimum and maximum were computed to visualize the morphological variation (see Supplementary I: Figures S2–-S6). To estimate the possibly different allometric trends we performed the regression of shape on size, with the CAC method (*plotAllometry* function in "geomorph"): the resulting common allometric component of shape data provides an estimation of the average allometric trends within groups (see in Mitteroecker et al., 2004; Klingenberg, 2016).

Moreover, to estimate the influence of the common evolutionary history of the studied species on the morphology of their bones, a multivariate K statistic (Kmult) analysis was performed (Table 3) using "phylocurve" package in R, based on the PC-scores and a composite phylogenetic tree (Figure 1) built in the Mesquite software (Maddison & Maddison, 2021). This composite phylogenetic tree (all branch lengths set to one) was built based on Jarvis et al. (2014) for the higher systematics, Gonzalez et al. (2009) for Anatidae, Friesen et al. (1996), and Moum et al. (2002) for Alcidae, and Bertelli and Giannini (2005) for Spheniscidae. Kmult measures the phylogenetic signal by comparing the observed rate of morphological trait variation to the trait variation expected under Brownian motion (Adams, 2014; Blomberg et al., 2003). Given the discrepancies in phylogenetic relationships for birds, additional phylogenetic hypotheses to our composite tree were also considered. For this we used trees with branch lengths downloaded from BirdTree (birdtree.org) (Jetz et al., 2012; Rubolini et al., 2015). We downloaded two sets ($n = 1000$ for each) of random phylogenetic trees, using "Ericson All Species" for one and "Hackett All Species" for the other as backbone phylogeny (Ericson et al., 2006; Hackett et al., 2008). Then we created two consensus trees, one from each of the sets in Mesquite, which we used to perform the analysis (see Supplementary I: Table S2). A K value >1

TABLE 3 Values obtained for test of the phylogenetic signal (and thus averaged by species) and Pearson's product moment correlation test of allometric effect (between log-transformed centroid size and the first three principal components), for each bone. Significant results ($p < 0.01$) are shown in bold.

		Humerus	Radius	Ulna	Femur	Tibiotarsus
Phylogeny		**$K = 2.456$** **$p < 0.01$**	**$K = 2.151$** **$p < 0.01$**	**$K = 1.267$** **$p < 0.01$**	**$K = 0.628$** **$p < 0.01$**	**$K = 0.720$** **$p < 0.01$**
Size	PC1	$r = -0.027$ $p = 0.626$	$r = 0.088$ $p = 0.058$	$r = -0.022$ $p = 0.553$	**$r = 0.222$** **$p < 0.01$**	**$r = 0.387$** **$p < 0.01$**
	PC2	**$r = 0.567$** **$p < 0.01$**	**$r = 0.359$** **$p < 0.01$**	**$r = 0.607$** **$p < 0.01$**	**$r = 0.321$** **$p < 0.01$**	$r = 0.015$ $p = 0.244$
	PC3	$r = -0.030$ $p = 0.688$	$r = -0.033$ $p = 0.835$	$r = -0.008$ $p = 0.387$	$r = -0.035$ $p = 0.839$	$r = -0.020$ $p = 0.506$

Abbreviation: *K*, *K*-value; *p*, *p*-value; *r*, Pearson's correlation coefficient.

suggests more similarities between phylogenetically closer relatives than expected under Brownian motion. We also projected phylogeny (from Figure 1) into the morphospace—using the "phytools" package in R (Revell, 2012)—to map the morphological diversification and understand the shape changes along the branches (Sidlauskas, 2008).

Because a significant phylogenetic signal was found, we conducted PGLS (Phylogenetic Generalized Least Squares) regressions between shape and size (centroid size), and between shape and locomotor categories with the function *procD.pgls* (from "geomorph" package with 1000 iterations), to test the interaction of size and locomotion types on shape variation of limb bones. However, the limited sample size and the small number of species by locomotor groups may obstruct the reliability and relevance of the results. To that matter, we also conducted a multivariate K statistic analysis on size and a Phylogenetic D statistic on the categories of the locomotor classifications to evaluate if they were themselves carrying a significant phylogenetic signal. Phylogenetic D statistic (Fritz & Purvis, 2010) involves calculating the observed D value for a binary character on a tree and comparing it with the D value found using an equal number of simulations under each of two models: (I) Phylogenetic Randomness and (II) Brownian Model.

3 | RESULTS

3.1 | Allometry

Looking at the axes one by one, allometry occurs in each studied wing bone: a significant allometry occurs on the second principal component (with higher correlation coefficient values for the humerus and ulna; Table 3). However, when testing the covariation of shape on size for the whole shape data, the result is significant only for the ulna ($r = 0.216$, $p < 0.01$). Concerning the hindlimb bones, the first and second principal components of the femora are (slightly) correlated with centroid size, whereas only the first principal component is, for the tibiotarsi (Table 3). When testing on the whole shape data, both femur ($r = 0.170$, $p < 0.01$) and tibiotarsus ($r = 0.178$, $p < 0.01$) results are significant (Supplementary I: Figures S2–S6).

3.2 | Morphological variation in the humerus

Here we describe the first two principal components, which combined represent 92.3% of the total variance (Figure 2). PC1 (88.8% of variance) describes the differences between the flightless and solely wing-propelled Spheniscidae on the positive side, and the other families, which spread on the negative side with overlaps (Figure 2). The theoretical humerus shape on the positive side of the first axis can be described with a robust proximal epiphysis and enlarged caput humeri. Specimens on the positive side have a larger area for the intumescentia humeri. The opening of the fossa tricipitalis (bordered by the crus dorsale fossae and crus ventrale fossae) is enlarged and is shifted distocaudally. The most distal point of the crista deltopectoralis is strongly distally shifted. The proc. flexorius is distocaudally strongly elongated, while the caudal ridges of the epicondylus ventralis and dorsalis are highly extended proximally. The condyles on the distal epiphysis are shifted proximocranially; among them, the condylus dorsalis has a more proximal position. On the contrary, the negative side of this axis includes humeri with a more gracile proximal epiphysis and a smaller caput humeri. These specimens have an intumescentia humeri with a reduced area, and a fossa tricipitalis with a smaller and more proximocranially situated opening. The distalmost elongation of the crista deltopectoralis is more proximally placed. The distal condyles are distally placed; they are located close to each other near the line of the diaphysis. The caudal ridges of the epicondylus ventralis and dorsalis are shorter and less extended proximally.

PC2 (3.5% of the variance) separates the volant and solely foot-propelled *Podiceps cristatus* (Podicipedidae) (7 and 8) and *Phalacrocorax carbo* (Phalacrocoracidae) (17 and 18) on the negative side from the other families (Figure 2). Anatidae (both volant and flightless, foot- and wing-propelled species) and Spheniscidae are positioned

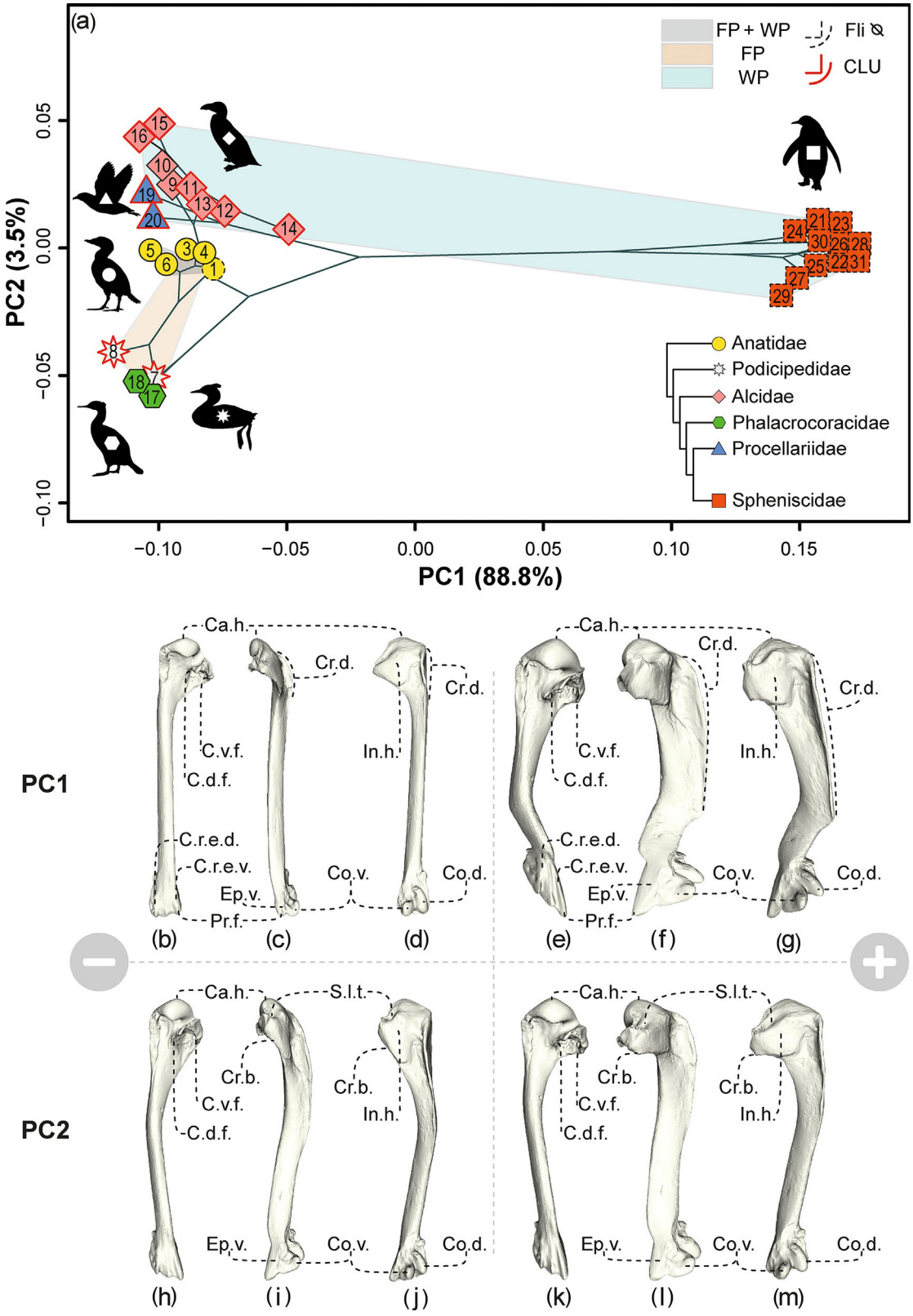

FIGURE 2 Legend on next page.

rather in the middle, while the volant and solely wing-propelled Procellariidae and Alcidae represent the most positive scores. The theoretical shape on the positive side shows humeri with a dorsoventrally wider proximal epiphysis besides a ventrally more extended intumescentia humeri and sulcus lig. transversus. The caput humeri is also more elongated dorsoventrally. The crista bicipitalis is less elongated distally but is more extended caudoventrally, and the opening of the fossa tricipitalis (bordered by the crus dorsale fossae and crus ventrale fossae) is shifted caudoventrally too. The distal condyles are situated somewhat more distocranially, while the distoventral region of the bone, including the epicondylus ventralis is more extended caudally. In contrast, the negative side contains specimens with a dorsoventrally less expanded proximal epiphysis, with a narrower intumescentia humeri and shorter sulcus lig. transversus. The caput humeri is also less expanded dorsoventrally. The crista bicipitalis is more elongated distally, but less extended caudoventrally, while the opening of the fossa tricipitalis is located more craniodorsally. The distal epiphysis is narrower, with a smaller distoventral region, and cranially less extended distal condyles. In the analysis with the penguins excluded, similar relative positions between the remaining families were obtained (Figure S18).

3.3 | Morphological variation in the radius

Here we describe the first two principal components, which together represent 89.4% of the overall variance (Figure 3). PC1 (85.1% of the variance) describes the separation of the flightless and solely wing-propelled Spheniscidae on the negative side, while the other families (both volant and flightless, foot- and wing-propelled species) are spreading from the center to the positive side (Procellariidae then Anatidae and Alcidae; Figure 3). The volant and solely foot-propelled Podicipedidae and Phalacrocoracidae have the most positive scores and are somewhat separated from the other specimens on the right side. Specimens with positive scores show a theoretical shape with a small cotyla humeralis with a rounded profile from the proximal view. The distal epiphysis is only moderately expanded caudocranially, while the distal area of the sulcus tendinosus occupies a significant area on it. Conversely, the theoretical shape with more negative scores represents a robust proximal epiphysis and extended cotyla humeralis (which is most expanded craniocaudally). The distal epiphysis is also highly expanded, as the facies articularis radiocarpalis is highly stretched in caudal and cranial directions, while the distal area of the sulcus tendinosus occupies only the central region.

The families spread along PC2 (4.3% of variance) with overlaps (Figure 3). The volant and solely foot-propelled Podicipedidae and Phalacrocoracidae have the most positive scores, while the other families have a rather central position, and the volant and solely wing-propelled Alcidae show the most negative values. Specimens on the positive side show a theoretical radius shape with more gracile epiphyses: with a small cotyla humeralis, and less extended facies articularis radiocarpalis. Specimens on the negative side have more robust epiphyses: larger cotyla humeralis, and a more extended facies articularis radiocarpalis. In the analysis with the penguins excluded, similar relative positions between the remaining families were obtained (Figure S19).

3.4 | Morphological variation in the ulna

Here we focus on the first three principal components, which together represent 87.4% of the overall variance (Figures 4 and 5). PC1 (46% of the variance) describes the differences between the flightless and solely wing-propelled Spheniscidae on the positive side, and the rest of the families on the negative side (Figure 4). Specimens on the negative side show a continuous transition with overlaps, with the Anatidae (both volant and flightless, foot- and wing-propelled species) and Alcidae (volant and solely wing-propelled) having the lowest scores, while Podicipedidae, Phalacrocoracidae (volant and solely foot-propelled), and Procellariidae (volant and solely wing-propelled) are positioned

FIGURE 2 (a) Principal component analyses plot of the first two principal components (PC1 and PC2) performed on the morphometric data of the humerus. Lines connecting the symbols indicate phylogeny mapping following Figure 1. Each symbol represents one specimen. Numbering is identical to Table 1 and the symbols follow Figure 1. Polygons and outlines display the locomotor categories following Table 2: FP, foot-propulsion; WP, wing-propulsion; FP + WP, both; CLU, clumsy (if not indicated, the specimen is mobile); Fli ⃠, flightless (if not indicated, the specimen is volant). (b–m) representation of the theoretical shapes based on the landmark configuration associated with the minimum (left) and maximum (right) values along PC1 (b–g) and PC2 (h–m). Directions are as follows: caudal, ventral, and cranial. Anatomical abbreviations: Ca.*h*., Caput humeri; *C.r.e.d*., Caudal ridge of epicondylus dorsalis; *C.r.e.v*., Caudal ridge of epicondylus ventralis; *Co.d*., Condylus dorsalis; *Co.v*., Condylus ventralis; *Cr.b*., Crista bicipitalis; *Cr.d*., Crista deltopectoralis; *C.d.f*., Crus dorsale fossae; *C.v.f*., Crus ventrale fossae; *Ep.v*., Epicondylus ventralis; *In.h*., Intumescentia humeri; *Pr.f*., Proc. flexorius; *S.l.t*., Sulcus lig. transversus.

closer to the center. The theoretical shape on the positive side shows ulnae that have large, caudocranially elongated cotyla ventralis which is facing proximally. The distal epiphysis is somewhat widened dorsoventrally, as there is a wider sulcus intercondylaris between the distal condyles, of which the ventral one

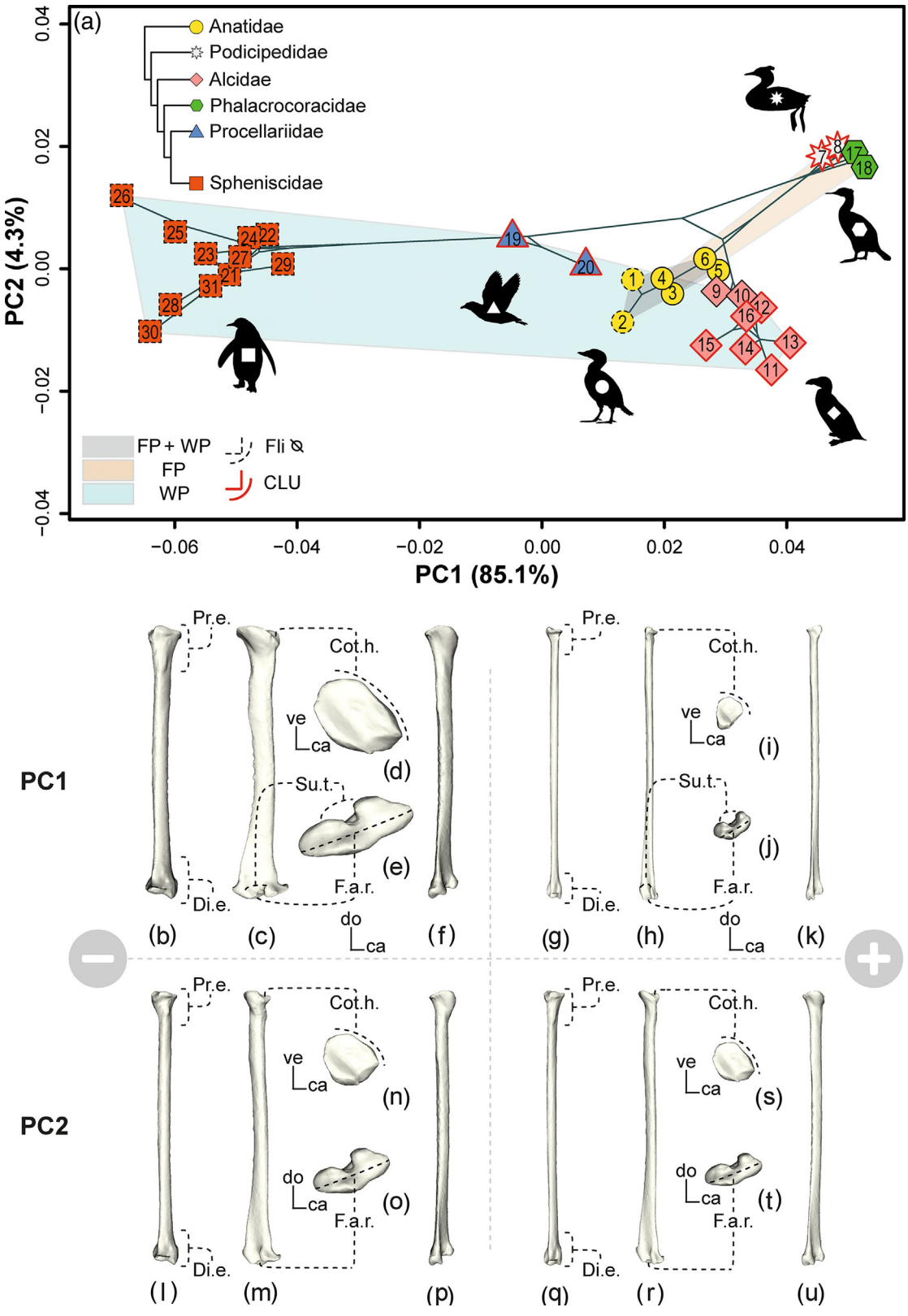

FIGURE 3 Legend on next page.

is notably elongated distoventrally. Contrary to this, the theoretical shape on the negative side shows ulnae with more proximocranially facing, and smaller cotyla ventralis, which is caudocranially less extended. It also shows a narrower sulcus intercondylaris, and a less elongated condylus ventralis.

PC2 (33% of the variance) separates the volant and solely foot-propelled Podicipedidae and Phalacrocoracidae on the positive side from the rest of the specimens on the opposing side which are spreading with overlaps (Figures 4 and 5). On the negative side the volant and solely wing-propelled Procellariidae, Alcidae, and the flightless wing-propelled *Spheniscus* specimens (27–29) show the lowest scores, while Anatidae and the rest of the penguins are positioned at the center. The theoretical shape associated with the positive side of this axis illustrates ulnae with gracile epiphyses, while the negative side shows more robust epiphyses, that are larger for a given length.

PC3 (8.4% of the variance) separates the species of volant and solely wing-propelled *Pelecanoides* (Procellariidae) (19 and 20) on the positive side from the other families (Figure 5) with Anatidae (both volant and flightless, foot- and wing-propelled species) showing the most negative values. The theoretical shape of specimens on the positive side presents a cotyla ventralis with a proximally elevated dorsal edge, while the ventral edge is located distally lower, which results in a cranioventral tilt and opening of the cotyla. On the negative side, the cotyla ventralis has a more elevated caudal and ventral edge, and a lower dorsal edge, which results in a cotyla that is less oriented ventrally, but more tilted in the proximocranial direction. In the analysis with the penguins excluded, similar relative positions between the remaining families were obtained (Figures S20 and S21).

A small bone, such as the ulna of the volant and solely wing-propelled *Pelecanoides* (19 and 20) and *Alle alle* (15 and 16) specimens is characterized by a more extended cotyla ventralis, and a dorsoventrally wider proximal epiphysis. In contrast, a large bone, like the ulna of the volant and solely foot-propelled *P. carbo* (17 and 18) shows a less extended cotyla ventralis, and dorsoventrally narrower proximal epiphysis (Figure S4).

3.5 | Morphological variation in the femur

The first three main components, which together represent 66.5% of the global variance, are described here (Figures 6 and 7). PC1 (40% of the variance) illustrates the differences between the *A. patagonicus* (mobile, solely wing-propelled, flightless: 21–24), *Mergus merganser* (mobile, wing- and foot-propelled, volant: 5 and 6), *P. carbo* (mobile, solely foot-propelled, volant: 17 and 18), and the solely foot-propelled but clumsy *P. cristatus* (7 and 8) specimens on the positive side, then Procellariidae and Alcidae (both solely wing-propelled and clumsy) on the negative side, while the rest of the Anatidae and Spheniscidae are situated rather in the middle (Figure 6). The first axis is mainly driven by robusticity: specimens on the positive side have larger, wider epiphyses, with enlarged caput femoris, a facies articularis antitrochanterica with a larger surface area, an elevated crista trochanteris, and a wider sulcus intercondylaris. Conversely, specimens on the negative side tend to have gracile epiphyses with small caput femoris, a facies articularis antitrochanterica with a significantly smaller surface area, a less prominent crista trochanteris, and a narrow sulcus intercondylaris.

PC2 (17% of the variance) separates the solely foot-propelled and clumsy *P. cristatus* (7 and 8), the solely wing-propelled and clumsy *Pelecanoides* (19 and 20), and to a lesser extent the solely foot-propelled but more mobile *P. carbo* (17 and 18) on the negative side from the solely wing-propelled and clumsy alcids, and the mobile spheniscids, and anatids (wing- and foot-propelled) (Figures 6 and 7), which spread along the positive side with overlaps (with the highest scores for spheniscids, and lowest for alcids). On the positive side of PC2, we can see bones characterized by a proximally elevated trochanter femoris, and saddle-shaped facies articularis antitrochanterica. Besides, the femora on the positive side have distally elongated crista trochanteris, and a narrow trochlea fibularis. The condylus lateralis and medialis are of similar size. In contrast, the theoretical shape of the specimens on the negative

FIGURE 3 (a) Principal component analyses plot of the first two principal components (PC1 and PC2) performed on the morphometric data of the radius. Lines connecting the symbols indicate phylogeny mapping following Figure 1. Each symbol represents one specimen. Numbering is identical to Table 1 and the symbols follow Figure 1. Polygons and outlines display the locomotor categories following Table 2: FP, foot-propulsion; WP, wing-propulsion; FP + WP, both; CLU, clumsy (if not indicated, the specimen is mobile); Fli ⃠, flightless (if not indicated, the specimen is volant). (b–u) representation of the theoretical shape based on the landmark configuration associated with the minimum (left) and maximum (right) values along PC1 (b–k) and PC2 (l–u). Directions are as follows: caudal, dorsal, proximal, distal, and cranial. Proximal (d, i, n, s) and distal (e, j, o, t) views are 2× magnified: ca, ve, and do indicate the caudal, ventral, and dorsal directions for them. Anatomical abbreviations: *Cot.h.*, Cotyla humeralis; *Di.e.*, Distal epiphysis; *F.a.r.*, Facies articularis radiocarpalis; *Pr.e.*, Proximal epiphysis; *Su.t.*, Sulcus tendinosus.

side of PC2 shows a mediolaterally elongated caput femoris, and a craniocaudally narrow, mediolaterally longer, flat facies articularis antitrochanterica, and short trochanter femoris. They have distally less elongated crista trochanteris and wide trochlea fibularis. The condylus lateralis is robust.

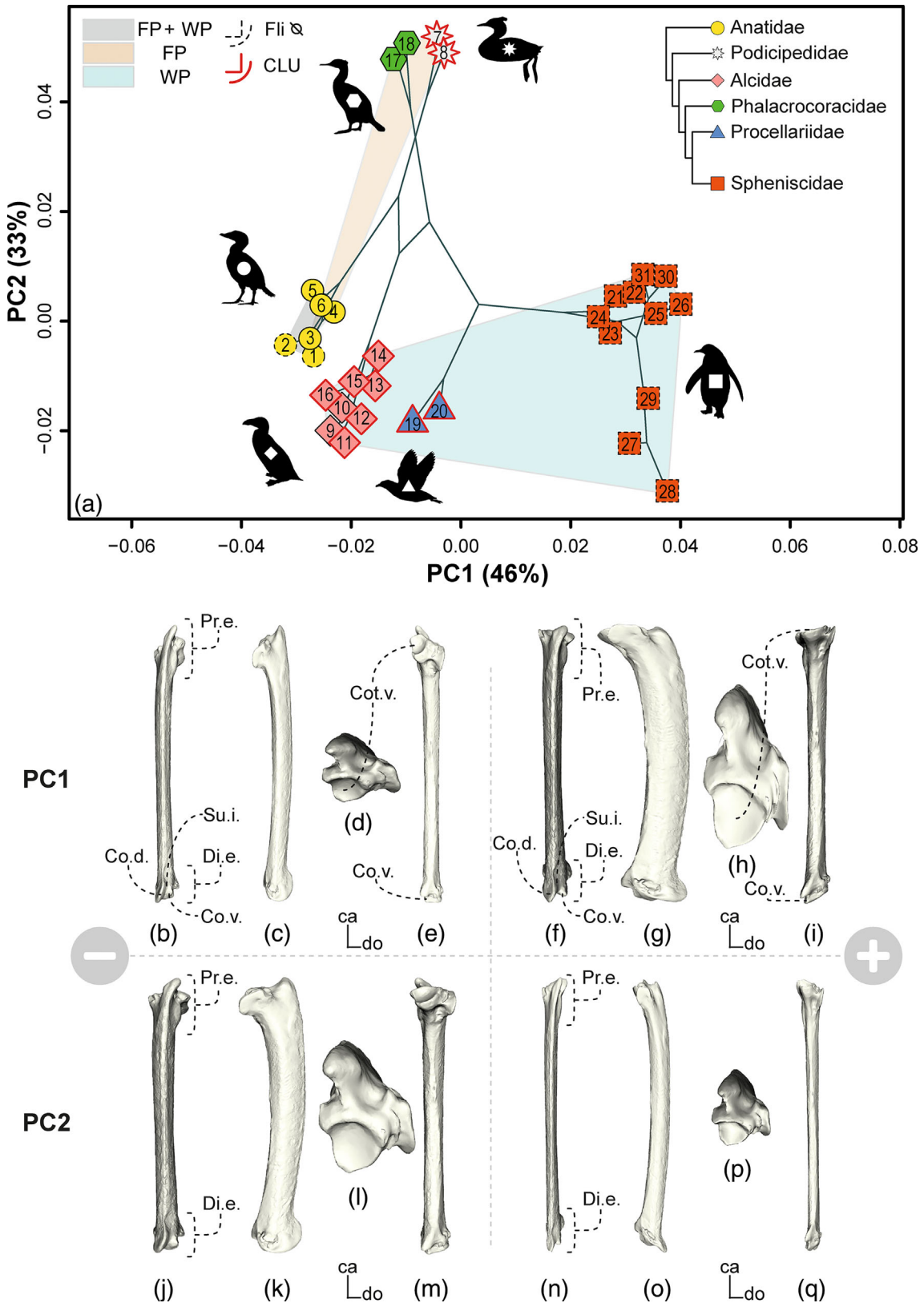

FIGURE 4 Legend on next page.

The PC3 axis (9.5% of the variance) highlights the difference between Podicipedidae on the positive side, and Phalacrocoracidae (both solely foot-propelled, but *P. carbo* is more mobile) on the negative side (Figure 7). The theoretical shape on the positive side represents bones with a distomedially pointing caput femoris. The distal condyles are positioned distally almost at the same level. On the negative side, the caput femoris points proximomedially, and the medial condyle is positioned more proximally than the lateral.

A small bone, such as the femur of the volant, solely wing-propelled and clumsy *Pelecanoides* (19 and 20) and *A. alle* (15 and 16) specimens is characterized by a caudocranially more extended proximal epiphysis and facies articularis antitrochanterica. In contrast, a large bone, such as the femur of the flightless, solely wing-propelled and mobile *A. patagonicus* (21–24) shows a mediolaterally more prolonged proximal epiphysis, with a medially more extended femoral head (Figure S5).

3.6 | Morphological variation in the tibiotarsus

Here we describe the first three components, which together represent 75.7% of the overall variance (Figures 8 and 9). PC1 (38% of the variance) clearly distinguishes between the flightless, mobile and solely wing-propelled Spheniscidae, the volant and also mobile Phalacrocoracidae (solely foot-propelled), and mobile Anatidae (both volant and flightless, foot- and wing-propelled species) on the negative side, and the clumsy Podicipedidae (solely foot-propelled), Alcidae, and the Procellariidae (solely wing-propelled) on the positive side (Figure 8). Penguins have the most negative scores, in the proximity of cormorants (17–18), while anatids are closer to the center. Alcids represent the lowest positive scores—with the outstanding low score of the mobile *Fratercula arctica* (10)—while the *Pelecanoides* (19 and 20) and *P. cristatus* (7 and 8) specimens have the highest values. The morphological differences, that affect the separation along the first axis mainly distinguish gracility versus robusticity. The theoretical shape on the positive side shows a tibiotarsus with small epiphyses, a proximally upward elongated cnemial crest with a narrow sulcus intercnemialis, and a proximal articular surface with a rather small area. The distal condyles are small, and the trochlea is narrow. In contrast, the negative side represents a tibiotarsus with robust, wider epiphyses, and wider sulcus intercnemialis. On the negative side, the proximal articular surface has a larger area, and the cnemial crest is elongated more into the proximocranial direction. The distal condyles are large, and the trochlea is broad.

PC2 accounts for 24.1% of the variation and clearly separates the solely foot-propelled and clumsy *P. cristatus* (Podicipedidae) specimens (7 and 8), on the positive side, from the other families which spread rather in the center and towards the negative side with overlaps (Figures 8 and 9). On the negative side most Alcidae (except 16), and *Anas penelope* (3 and 4) within Anatidae represent the lowest scores. The other anatids and most Spheniscidae are located rater in the middle. Among penguins, the *Spheniscus* (28 and 29) specimens are separated to some extent with more positive scores, with the *Pelecanoides* (19 and 20) and *P. carbo* (17 and 18) specimens. The theoretical shape on the positive side of the second axis represents a proximally strongly elongated cnemial crest, a laterally extended, but caudocranially short proximal articular surface, and a distally shifted crista fibularis. On the negative side, the cnemial crest is short, the proximal articular surface is more extended caudally, and the crista fibularis is proximally placed.

PC3 represents 13.6% of the variation and separates the mobile Anatidae (both wing- and foot-propelled) and mobile, solely foot-propelled Phalacrocoracidae on the positive side, from the other families on the negative side (Figure 9). Within anatids, *A. penelope* (3 and 4) shows particularly low scores. Specimens on the negative side are spreading along the axis with overlaps. The positive side of PC3 shows a theoretical shape with a wider crista fibularis, cranially extended condylus medialis, and an enlarged facies articularis medialis. The incisura intercondylaris is widened, and the distal condyles are somewhat medially oriented. On this side, the crista cnemialis

FIGURE 4 (a) Principal component analyses plot of the first two principal components (PC1 and PC2) performed on the morphometric data of the ulnae. Lines connecting the symbols indicate phylogeny mapping following Figure 1. Each symbol represents one specimen. Numbering is identical to Table 1 and the symbols follow Figure 1. Polygons and outlines display the locomotor categories following Table 2: FP, foot-propulsion; WP, wing-propulsion; FP + WP, both; CLU, clumsy (if not indicated, the specimen is mobile); Fli ⃠, flightless (if not indicated, the specimen is volant). (b–q) representation of the theoretical shape based on the landmark configuration associated with the minimum (left) and maximum (right) values along PC1 (b–i) and PC2 (j–q). Directions are as follows: caudal, dorsal, proximal, and cranial. Proximal (d, h, l, p) views are 2× magnified: ca and do indicate the caudal and dorsal directions for them. Anatomical abbreviations: *Co.d.*, Condylus dorsalis; *Co.v.*, Condylus ventralis; *Cot.v.*, Cotyla ventralis; *Di.e.* Distal epiphysis; *Pr.e.*, Proximal epiphysis; *Su.i.*, Sulcus intercondylaris.

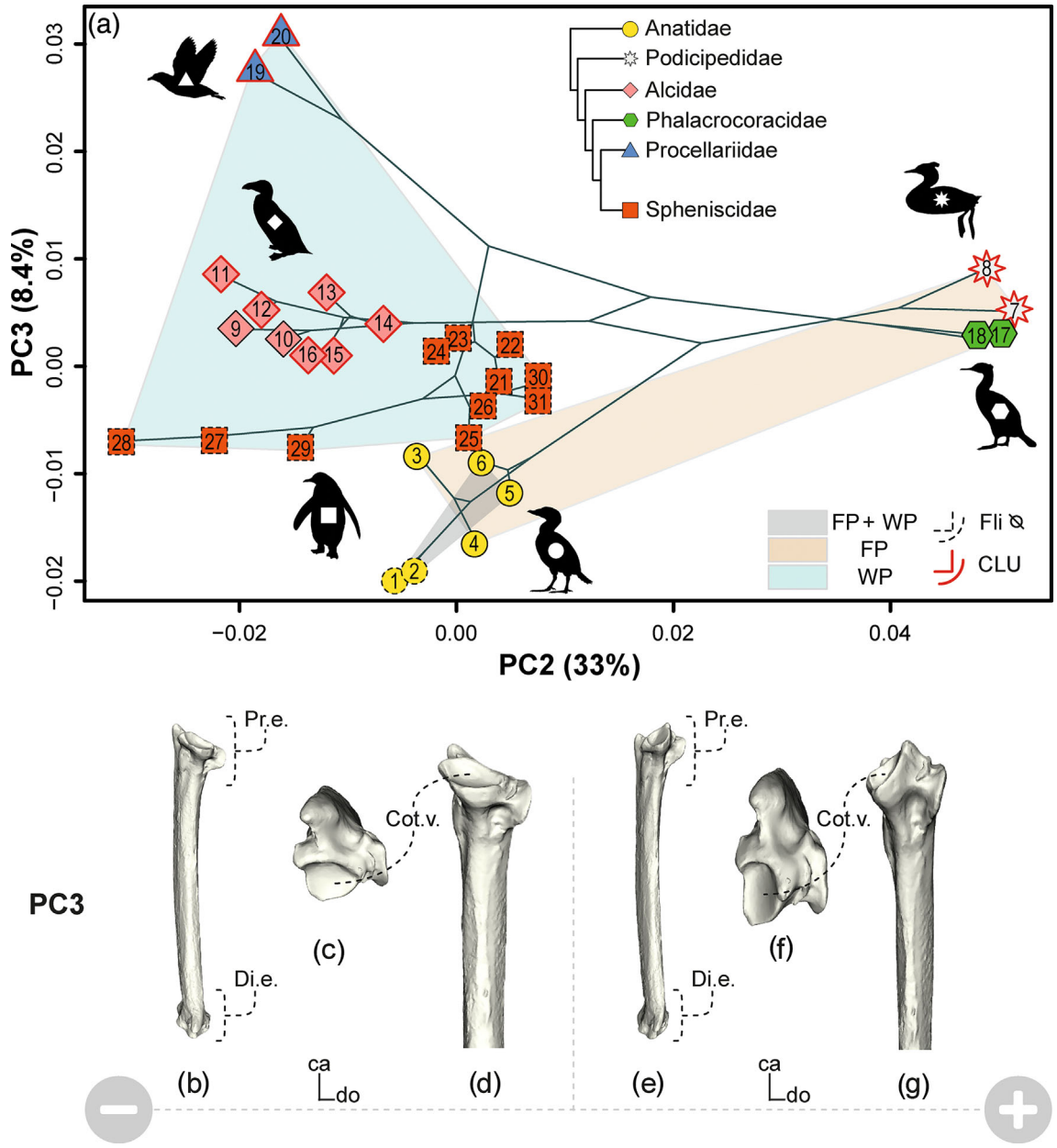

FIGURE 5 (a) Principal component analyses plot of the second and third principal components (PC2 and PC3) performed on the morphometric data of the ulnae. Lines connecting the symbols indicate phylogeny mapping following Figure 1. Each symbol represents one specimen. Numbering is identical to Table 1 and the symbols follow Figure 1. Polygons and outlines display the locomotor categories following Table 2: FP, foot-propulsion; WP, wing-propulsion; FP + WP, both; CLU, clumsy (if not indicated, the specimen is mobile); Fli ⊘, flightless (if not indicated, the specimen is volant). (b–g) representation of the theoretical shape based on the landmark configuration associated with the minimum (left) and maximum (right) values along PC3. Directions are as follows: ventrocranial, proximal, and cranial. Proximal (c, f) and cranial (d, g) views are 2× magnified. Ca and do indicates the caudal and dorsal directions for the proximal views. Anatomical abbreviations: *Cot.v.*, Cotyla ventralis; *Di.e.*, Distal epiphysis; *Pr.e.*, Proximal epiphysis.

cranialis is strongly overhanging cranially, while the crista cnemialis lateralis is strongly extended into the lateral direction. On the negative side, the crista fibularis is shorter, the condylus medialis is less extended cranially, and the facies articularis medialis has a smaller area. The incisura intercondylaris is narrow, and the distal condyles are parallel to the diaphysis. The crista cnemialis cranialis and lateralis are less extended cranially and laterally.

A small bone, such as the tibiotarsus of the volant, solely wing-propelled and clumsy *Pelecanoides* (19 and 20) and *A. alle* (15 and 16) specimens is characterized by

caudocranially narrow epiphyses and a caudocranially short proximal articular surface. In contrast, a large bone, such as the tibiotarsus of the flightless, solely wing-propelled and mobile *A. patagonicus* (21–24) shows caudocranially more extended epiphyses and a caudocranially more elongated proximal articular surface (Figure S6).

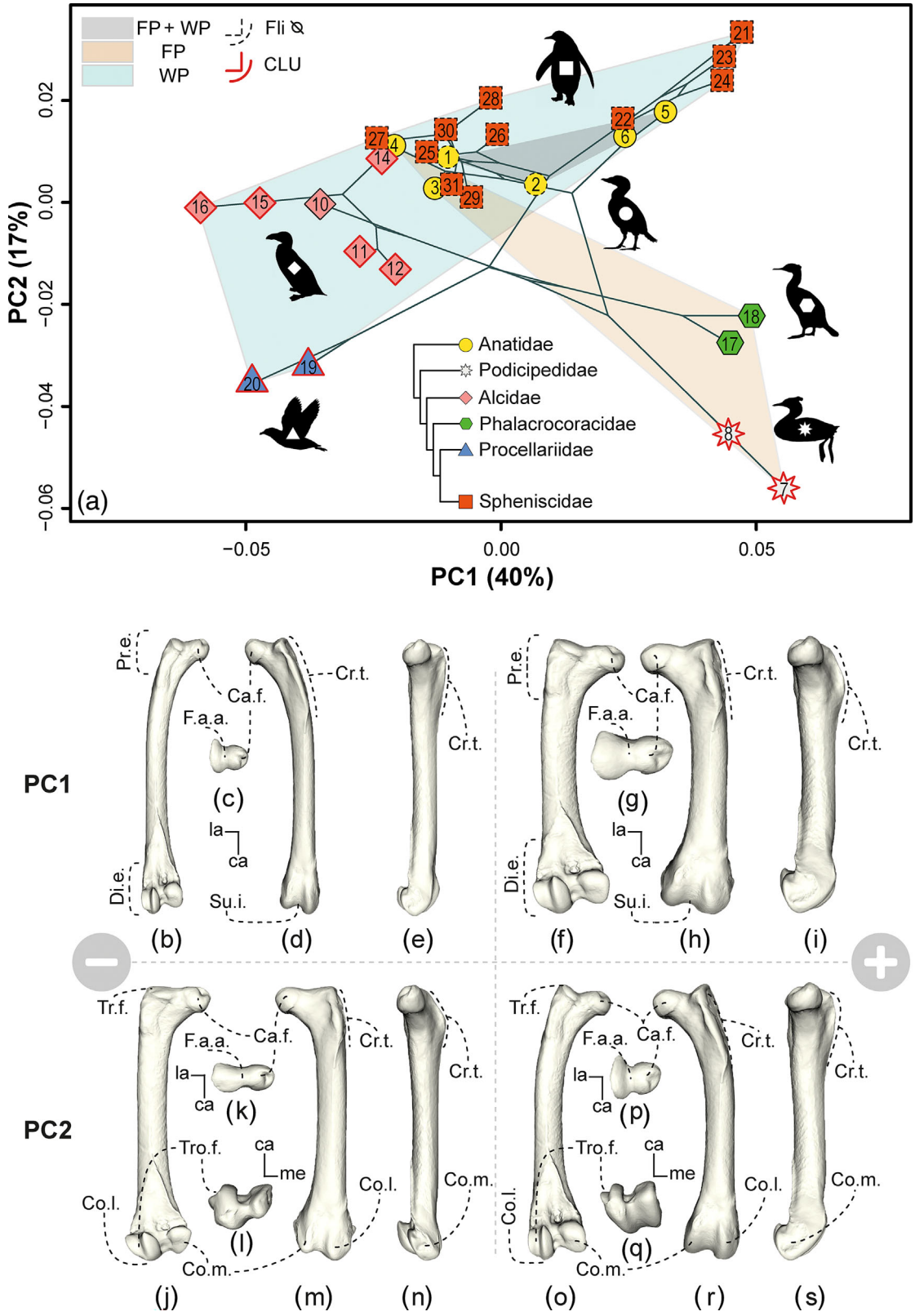

FIGURE 6 Legend on next page.

3.7 | Phylogenetic signal

Similar results were obtained using both our composite phylogenetic tree (Figure 1) and the two trees obtained from BirdTree. A strong influence of the phylogenetic history occurs on the morphology of every studied wing element, with K values >1 (especially for the humerus and radius) showing that the morphology of the bones of closer relatives is more similar than expected under Brownian motion (Adams, 2014; Blomberg et al., 2003). The analysis indicates a lower phylogenetic signal for the femora and tibiotarsi ($K < 1$) than predicted under Brownian motion (Table 3; Table S2). PGLS no longer reveals allometry in the shape of all bones, except the ulna, when phylogeny is taken into account (Table 4). However, size is strongly correlated with phylogeny in our sample, which may well account for this result (Table 5).

3.8 | Classification success based on locomotion types

Correct classification with the *k*-NN algorithm reached and exceeded 90% (varying between 89.6% and 100%) while predicting the use of foot-propulsion (Table 2) regarding the wing bones (Figure 10). Predicting the presence of wing-propulsion, and aerial skills also reached 90% for wing bones (ranging between 91.0%–93.5%, and 93.1%–96.7%, respectively), while the categorization based on terrestrial abilities drops to 79.3%–84.9%. For femora, the classification rate reaches 83.4% and 82.3% for the prediction of the presence of wing-propulsion and terrestrial skills, respectively, whereas it drops to 65.5% and 74.1%, based on the foot-propulsion categories and aerial abilities, respectively. In the case of the tibiotarsus, predicting terrestrial skill reached 96.6%, and foot-propulsion reached 93.5%, whereas predicting wing-propulsion and aerial skills dropped to 84.8% and 85.0%, respectively (Figure 10).

Considering the established baselines, the categorization based on the aerial abilities yielded the highest incidence of success for each wing bone, followed by categorization based on the presence of foot-propulsion, while categorization based on wing-propulsion and terrestrial abilities were the least successful. For the femur the categorization based on aerial and terrestrial capabilities resulted in the highest incidence of success and the classification based on the presence of wing- and foot-propulsion showed limited success. For the tibiotarsus the grouping based on terrestrial capabilities (closely followed by that based on foot-propulsion and aerial abilities) resulted in the highest efficiency, and the categorization based on wing-propulsion was the least successful (Figure 10).

The PGLS indicated that once phylogeny is taken into consideration, the shape is not associated with locomotion types, except for the ulna, where it is significantly correlated with the aquatic propulsive techniques (i.e., the presence or absence of foot- and wing-propulsion) (Table 6). However, the locomotor categories revealed a strong relationship with phylogeny, in our sample, biasing this result (Table 7). The estimated D is negative in every case, indicating some level of phylogenetic conservatism, while the low probability of E(D) resulting from no phylogenetic structure (close to 0) suggests a significant phylogenetic signal. The high probability of E(D) resulting from Brownian phylogenetic structure (close to 1) suggests that the observed pattern can be explained by a Brownian process. Overall, these results suggest that the binary categories of our locomotor classifications (Table 2) exhibit a significant phylogenetic signal, and the pattern is consistent with a Brownian motion process. Therefore, the fact that trying to remove the impact of phylogeny nullifies the significance of the link between locomotor categories and shape may be strongly influenced by the fact that the functional and phylogenetic signals are strongly mixed in our sample (Table 7).

4 | DISCUSSION

4.1 | Phylogenetic history

With regard to the wing bones, the phylogenetic signal is strong, and there seems to always be a clear separation of

FIGURE 6 (a) Principal component analyses plot of the first two principal components (PC1 and PC2) performed on the morphometric data of the femora. Lines connecting the symbols indicate phylogeny mapping following Figure 1. Each symbol represents one specimen. Numbering is identical to Table 1 and the symbols follow Figure 1. Polygons and outlines display the locomotor categories following Table 2: FP, foot-propulsion; WP, wing-propulsion; FP + WP, both; CLU, clumsy (if not indicated, the specimen is mobile); Fli ⃠, flightless (if not indicated, the specimen is volant). (b–s) representation of the theoretical shape based on the landmark configuration associated with the minimum (left) and maximum (right) values along PC1 (b–i) and PC2 (j–s). Directions for PC1: caudal, proximal, cranial and medial. Directions for PC2: caudal, proximal, distal, cranial and medial. Ca, la, and me indicates the caudal, lateral, and medial directions for the proximal (c, g, k, p) and distal (l, q) views. Anatomical abbreviations: Ca.*f.*, Caput femoris; *Co.l.*, Condylus lateralis; *Co.m.*, Condylus medialis; *Cr.t.*, Crista trochanteris; *Di.e.*, Distal epiphysis; *F.a.a.*, Facies articularis antitrochanterica; *Pr.e.*, Proximal epiphysis; *Su.i.*, Sulcus intercondylaris; *Tr.f.*, Trochanter femoris; *Tro.f.*, Trochlea fibularis.

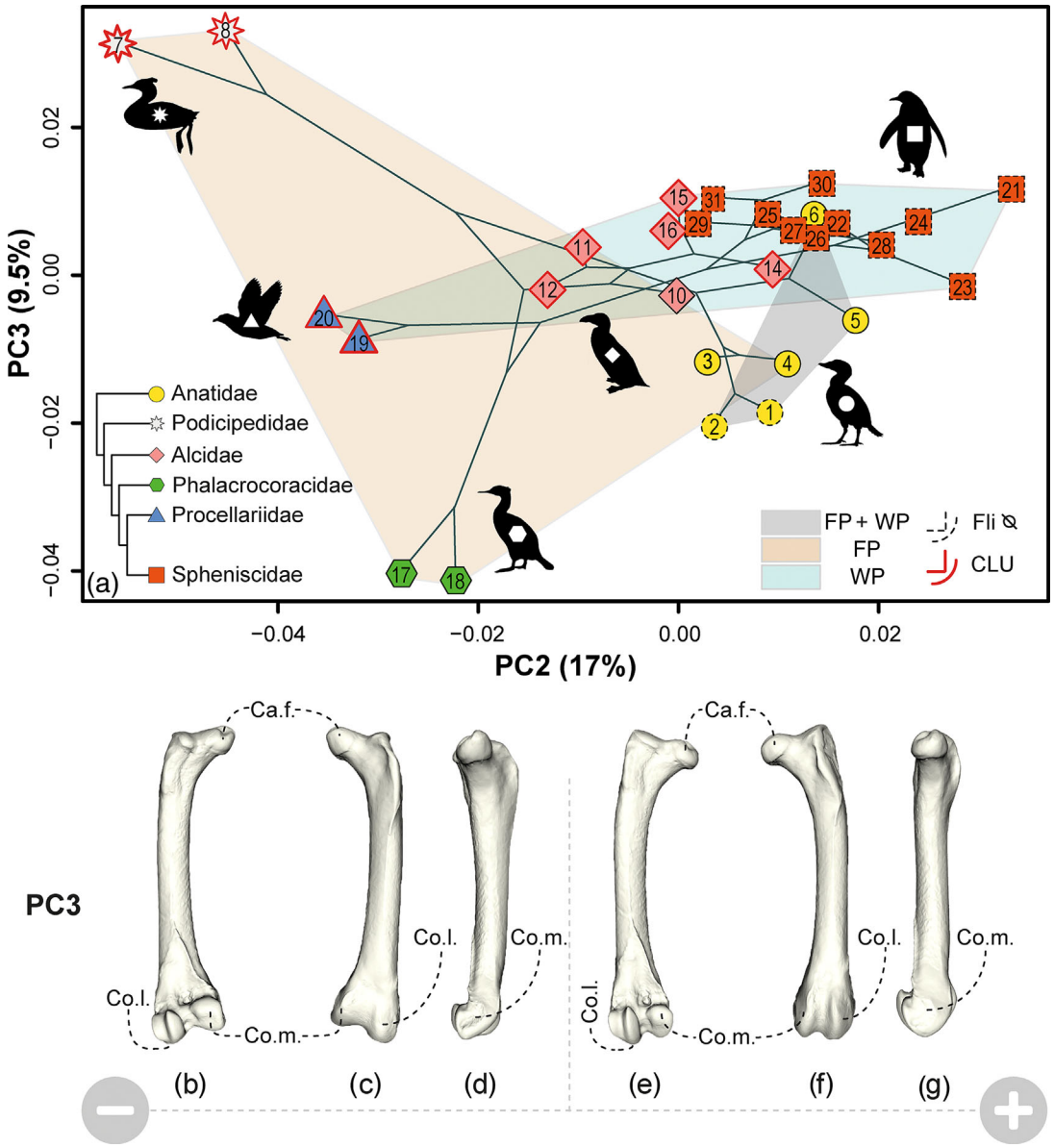

FIGURE 7 (a) Principal component analyses plot of the second and third principal components (PC2 and PC3) performed on the morphometric data of the femora. Lines connecting the symbols indicate phylogeny mapping following Figure 1. Each symbol represents one specimen. Numbering is identical to Table 1 and the symbols follow Figure 1. Polygons and outlines display the locomotor categories following Table 2: FP, foot-propulsion; WP, wing-propulsion; FP + WP, both; CLU, clumsy (if not indicated, the specimen is mobile); Fli ⃠, flightless (if not indicated, the specimen is volant). (b–g) representation of the theoretical shape based on the landmark configuration associated with the minimum (left) and maximum (right) values along PC3. Directions are as follows: caudal, cranial and medial. Anatomical abbreviations: Ca.*f.*, Caput femoris; *Co.l.*, Condylus lateralis; *Co.m.*, Condylus medialis.

the families. The strongest phenotypic divergence separates the Spheniscidae from the other families (to a lesser extent for the ulna). This could highlight the specific ecology of this family (well-adapted wing-propelled, but flightless) and the extreme morphology of their wing bones, as well as the general conservatism of wing bone shape within each family. However, some of the families constantly group under morphological similarity despite their distant phylogenetic relationship, such as members of the Anatidae, Alcidae, and Procellariidae. Similarly, the also distantly related Phalacrocoracidae and Podicipedidae (foot-propelled, that do not apply wing-propulsion) also group together. In contrast, the consistently large morphological difference between the otherwise closely related Spheniscidae and Procellaridae is striking and can highlight specific functional requirements resulting

from their different ecologies, since both families are wing-propelled, but the Procellaridae are volant and their wings must be capable of aerial movements too. In our sample, besides the penguins, *Tachyeres pteneres* is also flightless and also has a specialized wing-assisted aquatic behavior, however, the morphology of its wing bones still

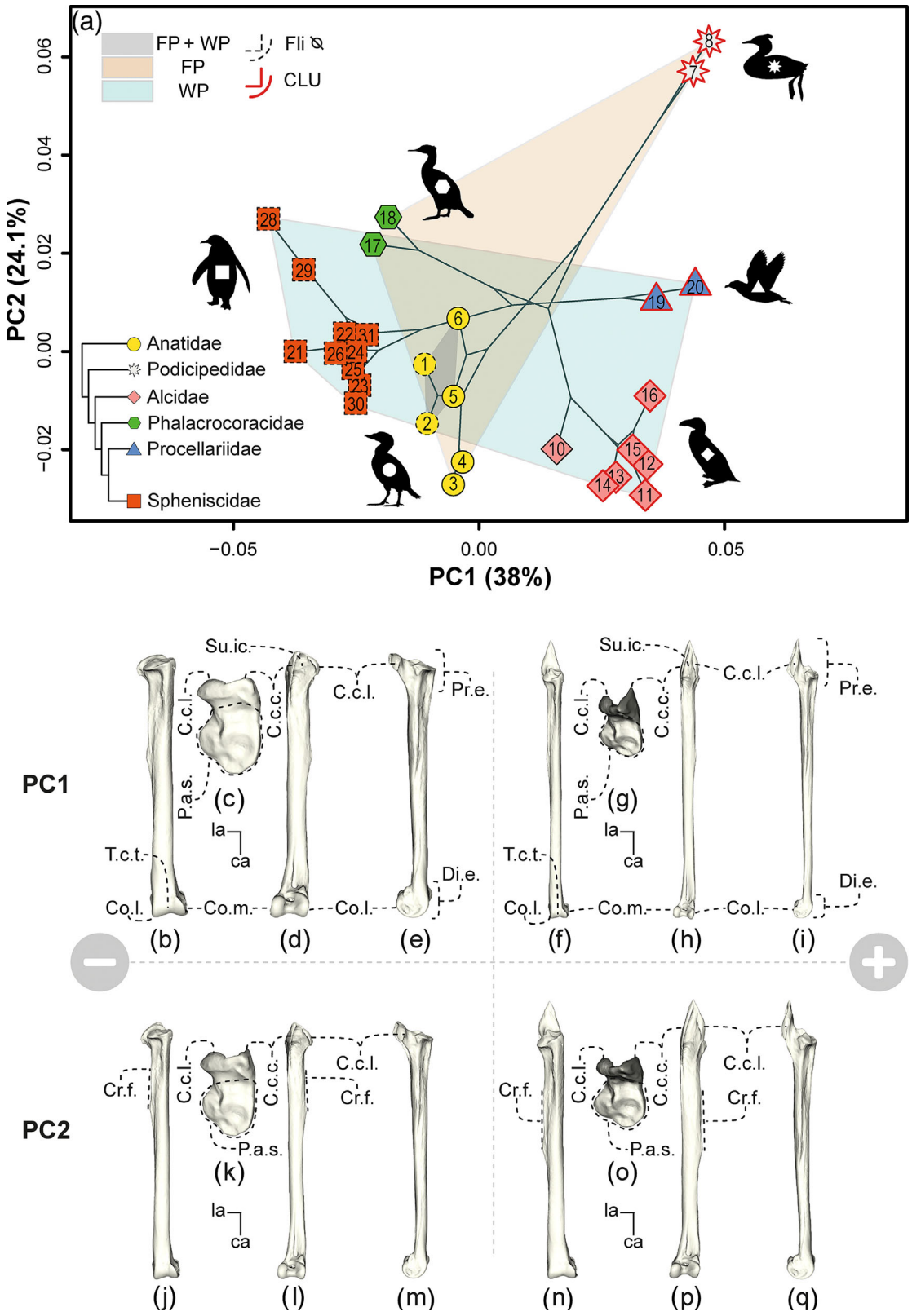

FIGURE 8 Legend on next page.

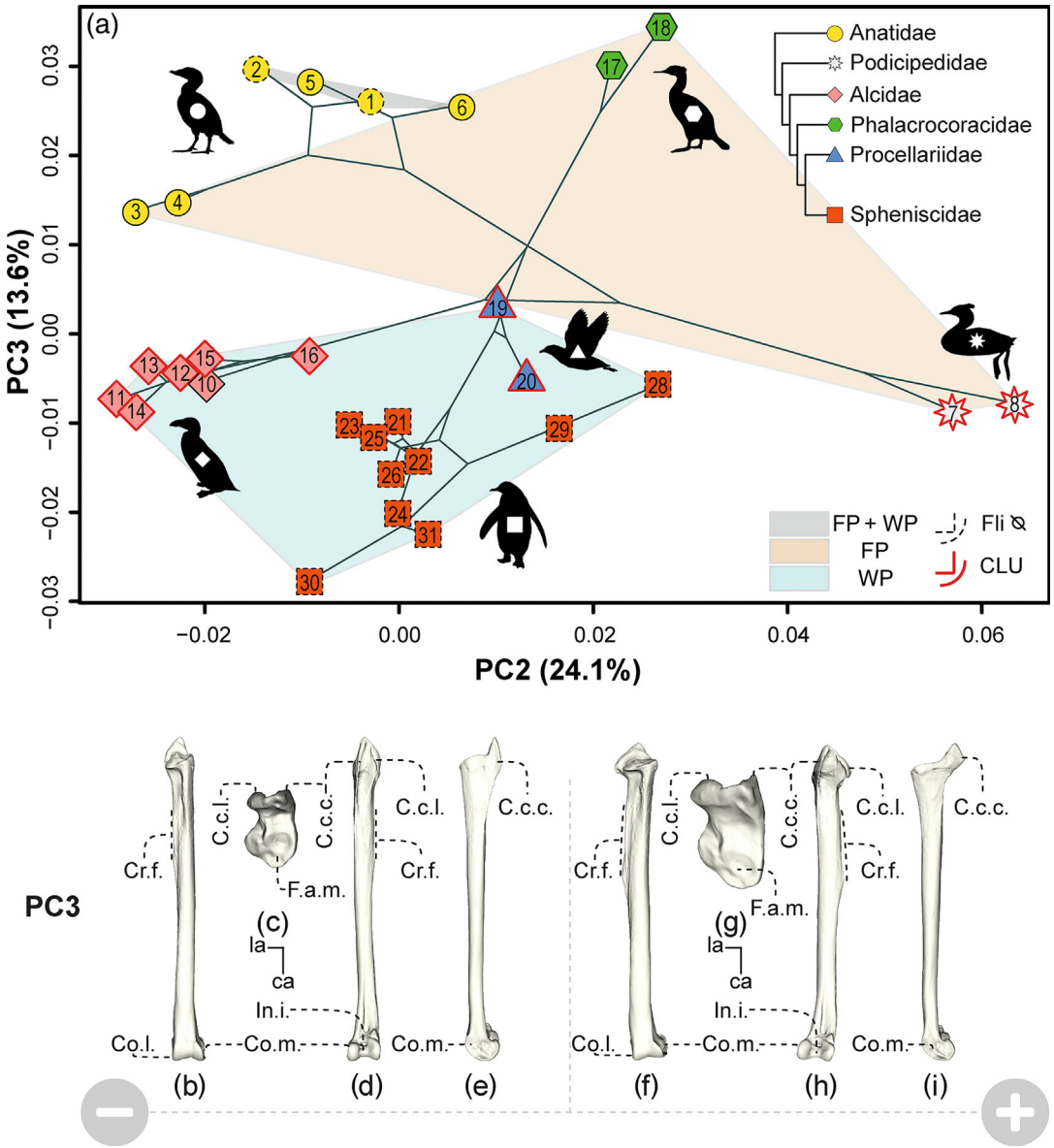

FIGURE 9 (a) Principal component analyses plot of the second and third principal components (PC2 and PC3) performed on the morphometric data of the tibiotarsi. Lines connecting the symbols indicate phylogeny mapping following Figure 1. Each symbol represents one specimen. Numbering is identical to Table 1 and the symbols follow Figure 1. Polygons and outlines display the locomotor categories following Table 2: FP, foot-propulsion; WP, wing-propulsion; FP + WP, both; CLU, clumsy (if not indicated, the specimen is mobile); Fli ⃠, flightless (if not indicated, the specimen is volant). (b–i) representation of the theoretical shape based on the landmark configuration associated with the minimum (left) and maximum (right) values along PC3. Directions are as follows: caudal, proximal, cranial and medial. Proximal views (c, g) are 2× magnified, ca and la indicates the caudal and lateral direction for them. Anatomical abbreviations: *C.c.c.*, Crista cnemialis cranialis; *C.c.l.*, Crista cnemialis lateralis; *Co.l.*, Condylus lateralis; *Co.m.*, Condylus medialis; *Cr.f.*, Crista fibularis; *F.a.m.*, Facies articularis medialis; *In.i.*, Incisura intercondylaris.

FIGURE 8 (a) Principal component analyses plot of the first two principal components (PC1 and PC2) performed on the morphometric data of the tibiotarsi. Lines connecting the symbols indicate phylogeny mapping following Figure 1. Each symbol represents one specimen. Numbering is identical to Table 1 and the symbols follow Figure 1. Polygons and outlines display the locomotor categories following Table 2: FP, foot-propulsion; WP, wing-propulsion; FP + WP, both; CLU, clumsy (if not indicated, the specimen is mobile); Fli ⃠, flightless (if not indicated, the specimen is volant). (b–q) representation of the theoretical shape based on the landmark configuration associated with the minimum (left) and maximum (right) values along PC1 (b–i) and PC2 (j–q). Directions are as follows: caudal, proximal, cranial, and lateral. Proximal views (c, g, k, o) are 2× magnified, ca and la indicates the caudal and lateral direction for them. Anatomical abbreviations: *C.c.c.*, Crista cnemialis cranialis; *C.c.l.*, Crista cnemialis lateralis; *Co.l.*, Condylus lateralis; *Co.m.*, Condylus medialis; *Cr.f.*, Crista fibularis; *Di.e.*, Distal epiphysis; *P.a.s.*, Proximal articular surface; *Pr.e.*, Proximal epiphysis; *Su.ic.*, Sulcus intercnemialis; *T.c.t.*, Trochlea cartilaginis tibialis.

resembles that of other anatids. This can be linked to the rather recent appearance of flightlessness in the *Tachyeres* species, probably in glacial or post-glacial times (Fulton et al., 2012; Livezey, 1986), whereas flying abilities of penguins disappeared much earlier (probably already in the Palaeogene) (Ksepka & Ando, 2011); in addition, penguins are characterized by a much more specific mode of wing-propulsion (Hui, 1988).

TABLE 4 *p*-values for PGLS computed with the composite phylogenetic tree (Figure 1) on shape data and centroid size for each bone. Significant results ($p < 0.01$) are shown in bold.

Bone	*p*-value
Humerus	$p = 0.275$
Radius	$p = 0.278$
Ulna	$\mathbf{p = 0.001}$
Femur	$p = 0.394$
Tibiotarsus	$p = 0.733$

The phylogenetic signal is weaker for the hindlimb bones, and no family is clearly separated from the others. Though the specimens of a given family usually show strong morphological similarities, there are noteworthy exceptions for the femur, for which the spheniscid and anatid specimens are each separated into different groups related to different body mass (like e.g., the separation of the heavy *Aptenodytes* penguins from the lighter penguins) or locomotor ecology (like e.g., the split of the advanced foot-propelled *M. merganser* from the other anatids), respectively. However, such a split within these families is not present for the tibiotarsus. The terrestrially mobile Spheniscidae and clumsy Procellariidae, which are otherwise closely related, consistently represent strikingly different morphologies, probably related to their entirely different terrestrial abilities. Apparent on both hindlimb bones is the similar morphology of Alcidae and Procellariidae (even though they are not the closest relatives) probably because of their similarly reduced terrestrial capabilities. Both the femur and tibiotarsus show a certain degree

	Humerus	Radius	Ulna	Femur	Tibiotarsus
Phylogeny	$\mathbf{K = 0.967}$ $\mathbf{p < 0.01}$	$\mathbf{K = 1.004}$ $\mathbf{p < 0.01}$	$\mathbf{K = 0.989}$ $\mathbf{p < 0.01}$	$\mathbf{K = 1.281}$ $\mathbf{p < 0.01}$	$\mathbf{K = 1.025}$ $\mathbf{p < 0.01}$

TABLE 5 Values obtained for test of the phylogenetic signal in centroid size, for each bone. Significant results ($p < 0.01$) are shown in bold.

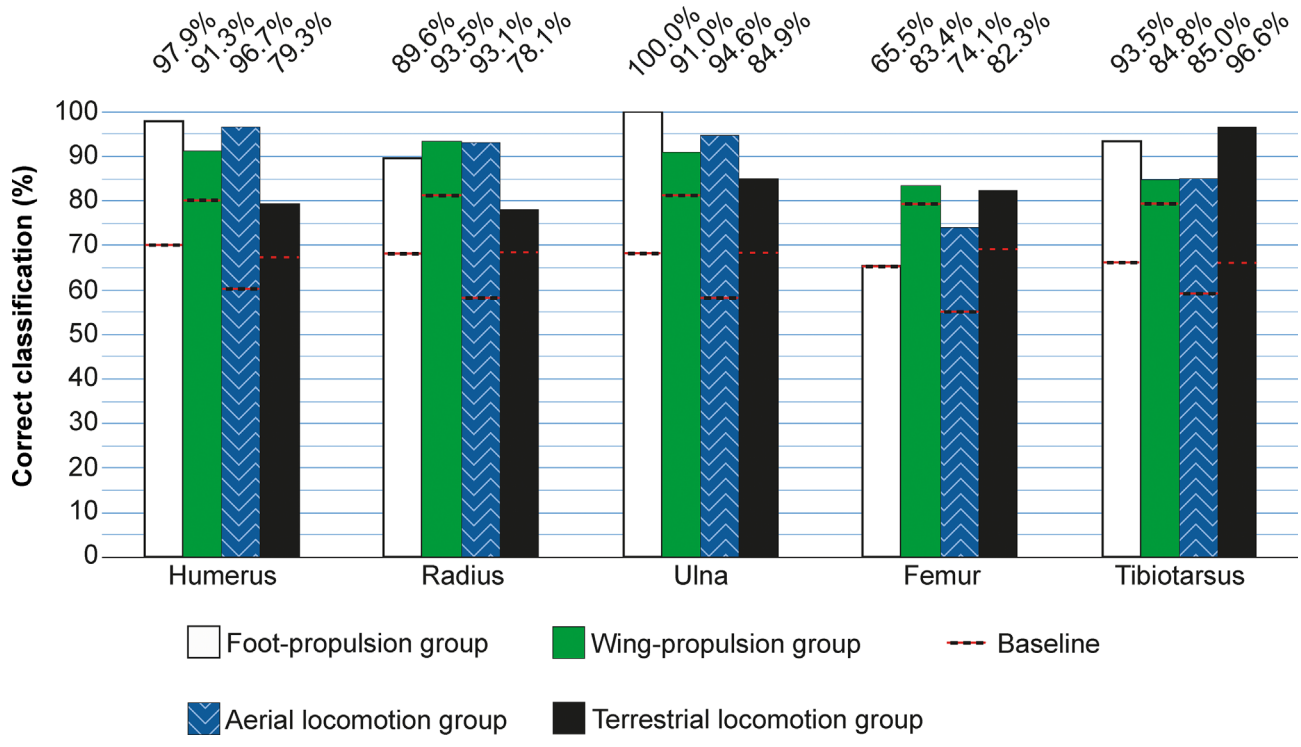

FIGURE 10 Percentage of correct predictions of aquatic, aerial, and terrestrial locomotion groups with the *k*-NN algorithm for each bone (see Table 2 for the categories). Dashed baselines for each column separate the possible extent to which the prediction success depends on morphological information (above the line), and the expected percentage of correct classification due to chance (below the line).

TABLE 6 *p*-values for PGLS computed with the composite phylogenetic tree (Figure 1) on shape data and categories of the locomotor classifications for each bone. Significant results ($p < 0.01$) are shown in bold.

Bone	Foot-propulsion present or not	Wing-propulsion present or not	Flying ability present or not	Terrestrial mobility present or not
Humerus	$p = 0.162$	$p = 0.358$	$p = 0.13$	$p = 0.364$
Radius	$p = 0.164$	$p = 0.317$	$p = 0.26$	$p = 0.573$
Ulna	$\mathbf{p = 0.001}$	$\mathbf{p = 0.001}$	$p = 0.064$	$p = 0.149$
Femur	$p = 0.219$	$p = 0.365$	$p = 0.44$	$p = 0.711$
Tibiotarsus	$p = 0.218$	$p = 0.363$	$p = 0.303$	$p = 0.508$

TABLE 7 Phylogenetic D statistic computed on the categories of the locomotor classifications with the composite phylogenetic tree (Figure 1).

Bone	Foot-propulsion present or not	Wing-propulsion present or not	Flying ability present or not	Terrestrial mobility present or not
Humerus	E(D): −1.4528 rand.: 0.0 Br.m.: 0.999	E(D): −0.8019 rand.: 0.002 Br.m.: 0.878	E(D): −1.3031 rand.: 0.0 Br.m.: 0.981	E(D): −1.0511 rand.: 0.0 Br.m.: 0.969
Radius	E(D): −1.4284 rand.: 0.0 Br.m.: 0.998	E(D): −0.7564 rand.: 0.0 Br.m.: 0.898	E(D): −1.1928 rand.: 0.0 Br.m.: 0.993	E(D): −1.0783 rand.: 0.0 Br.m.: 0.959
Ulna	E(D): −1.4390 rand.: 0.0 Br.m.: 0.998	E(D): −0.7622 rand.: 0.001 Br.m.: 0.884	E(D): −1.2699 rand.: 0.0 Br.m.: 0.99	E(D): −1.0786 rand.: 0.0 Br.m.: 0.976
Femur	E(D): −1.4010 rand.: 0.0 Br.m.: 0.999	E(D): −0.7297 rand.: 0.001 Br.m.: 0.861	E(D): −1.1563 rand.: 0.0 Br.m.: 0.981	E(D): −0.9840 rand.: 0.0 Br.m.: 0.954
Tibiotarsus	E(D): −1.4234 rand.: 0.0 Br.m.: 0.996	E(D): −0.7565 rand.: 0.002 Br.m.: 0.884	E(D): −1.2524 rand.: 0.0 Br.m.: 0.993	E(D): −1.0094 rand.: 0.0 Br.m.: 0.957

Abbreviations: Br.m., simulations under Brownian Model; E(D), estimated D; rand., simulations under phylogenetic randomness.

of morphological similarity in the phylogenetically distant but terrestrially similarly mobile penguins and ducks; however, this is more complex for the femur, since the *A. patagonicus* penguins are close to *M. merganser* together with (the also distant relative) advanced foot-propelled *P. cristatus* and *P. carbo* (Figure S16). On the contrary, the tibiotarsus of *P. cristatus* is the closest to the distantly related but similarly clumsy *Pelecanoides* specimens.

Our analysis revealed a robust influence of the phylogenetic background on the bones' morphology, size, but also on the locomotor behavior of the studied families. The important phylogenetic impact can be the result of the composition or size of our sample, although the presence of a considerable phylogenetic signal (with high *K* values close to or above 1) has been mentioned in previous studies on birds (Bell et al., 2021) in several anatomical regions: for instance, in the vertebral count (Böhmer et al., 2019), three-dimensional cranial morphology (Felice & Goswami, 2018), proportions of the main forelimb bones (Hinić-Frlog & Motani, 2010; Wang & Clarke, 2014), but also regarding the wing shape and limb bone morphology (Provini & Höfling, 2020; Serrano et al., 2020). Accordingly, although outstretched wing outline (including in aquatic taxa) correlates with foraging behavior, wing shape within a given clade shows major similarities (Baumgart et al., 2021; Wang & Clarke, 2015). Despite the limited size of our sample, and the difficulty raised by the mixed phylogenetic and functional signals, some functional adaptive features can be highlighted as the phylogenetic signal does not preclude the functional one.

4.2 | Functional adaptive features

The quantitative analysis did not confirm the relationship of morphology with locomotion when phylogeny is taken into account (except for the ulna for the aquatic propulsion techniques), yet particular trends can be observed in the

morphological variation, which might be related to functional adaptations to some extent.

The observed dorsoventral elongation of the proximal epiphysis and the ventral shift of the fossa tricipitalis in the volant WP taxa (Figure 2k–m) might be connected to the larger attachment of the triceps, as the fossa tricipitalis is an important attachment site for the triceps muscle (Baumel et al., 1993; Owre, 1967; Watanabe et al., 2021), whose main function is the extension of the elbow during down and up-strokes (Vazquez, 1994). In some wing-propelled groups (like in Alcidae and *Pelecanoides*) the origin of this muscle is enlarged: it extends dorsally, outside of the fossa (McKitrick, 1991; Watanabe et al., 2021), which might contribute to further stabilizing the wings during aquatic movements.

The robust and enlarged humeral head of the flightless wing-propelled penguins (Figure 2) might contribute to a more stable shoulder, since the humeral head serves as the articular surface in the shoulder joint (Jenkins, 1993), through which main motions take place during both aerial and aquatic "flight". In penguins, the fossa tricipitalis enlarges and deepens in accordance with the larger humeral head (Figure 2b–g). The main head of the triceps is attached deeply within the fossa similarly to in volant taxa, but it has an altered function in penguins: its main role is to stabilize and further stiffen the elbow (Haidr & Hospitaleche, 2017; Schreiweis, 1982; Watanabe et al., 2021). The most striking morphological change that distinguishes penguins from the other birds in our dataset is the extreme distal elongation of the crista deltopectoralis (Figure 2b–g). In penguins, the deltopectoral crest most of all serves as a leading edge, as along its cranial margin runs a long ligament (ligg. propatagiale et limitans cubiti), which may increase stability and stiffness (De Blois & Motani, 2019; Watanabe et al., 2021). This crest also carries ventrally the main attachment of the m. pectoralis (that strikes the upraised wing) (Watanabe et al., 2021), but the large crest (through the high caudo-cranial expansion of the humerus) may also contribute to increasing the attachment site for the m. supracoracoideus—which elevates the wing (Louw, 1992; Watanabe et al., 2021). In flying birds, the condylus dorsalis articulates with the ulna and radius, while the condylus ventralis articulates only with the ulna (Baumel et al., 1993). However, in penguins, the two distal condyles of the humerus are shifted and form two flat 'articular facets' (Louw, 1992): the dorsal condyle articulates only with the radius, whereas the ventral condyle articulates only with the ulna with decreased mobility. An additional anatomical feature associated with significantly reduced elbow mobility in penguins is the enlarged proc. flexorius (Figure 2e–g), which provides articulation for a large sesamoid, and thus further contributes to elbow stiffness (Haidr & Hospitalaleche, 2017). We observed that volant wing-propelled taxa show enlarged epiphyses on the radius and ulna: due to the greater forces acting on the wing, the somewhat more robust epiphyses might be functionally advantageous for the volant taxa that apply wing-propulsion (but this is also connected to the allometry observed—see below). The widened epiphyses of penguins are highly modified in addition to this, for both the radius and for the ulna (Figures 3 and 4). For this family the distal condyles of the humerus and the articular surfaces of the radius and ulna are flattened joint surfaces (instead of mobile joints), which stabilize the wing/flipper (Krahl & Werneburg, 2022; Raikow et al., 1988).

The exceptional proximal joint surface (Figure 5) on the ulna of *Pelecanoides* specimens may contribute to elbow stability: the cranioventrally facing cotyla ventralis might provide a better articulation with the condylus ventralis of the humerus (for example during the swimming with partially folded elbow). However, a better covering with surface landmarks in future studies could enable us to better characterize and understand this morphology.

The wing bones of Anatidae most closely resemble in our sample to those of the volant wing-propelled species. The morphological similarity between these three families is interesting, because although there are species within the Anatidae that use wing-propulsion, they are not nearly as well adapted to it as the Alcidae and Procellariidae. Since our landmarks are limited to the epiphyses, it is possible that some of the morphological differences associated with this adaptation (such as a flattened diaphysis) are not reachable in the present analysis.

Terrestrial species with a larger body mass (like *A. patagonicus*, *P. carbo*, and *M. merganser*), and *P. cristatus* with advanced foot-propulsion skills both show robust femora (Figure 6f–i). We hypothesize that this might be mechanically more suitable to resist the loadings associated with bearing a larger body, and with more intense foot-propulsion (but this is partly connected to the allometry observed on the femur—see below). A further potential functional similarity among heavy terrestrial and advanced foot-propelled birds is the presence of a powerful pelvic musculature that provides stability and connects the pelvis with the proximal femur (Clifton et al., 2018; Raikow, 1970; Schreiweis, 1982; Setty, 1959). The distal part of the femur also serves as an important attachment site for the muscles associated with the locomotion, which may also explain the robustness of the femur in heavier and advanced FP species. For example, the knee extensor muscles are exceptionally well-developed in advanced foot-propelled divers, such as in grebes (Clifton et al., 2018), but are also large in the case of penguins (Schreiweis, 1982; Setty, 1959). However, for penguins, it is probably not related to foot-propulsion,

but more to their vertically upright stance/walk. Other muscles that arise from the distal part of the femur and act as knee flexors and as ankle plantarflexors (Raikow, 1970; Schreiweis, 1982) also reach a large size in foot-propelled divers (Clifton et al., 2018). These large muscles provide stronger plantarflexion moments for foot-propelled birds, but they could also be beneficial on land, for example, when penguins are pushing themselves on ice/snow with their feet while laying on their belly. Although the femoral trochanter is a significant attachment site for the pelvic muscles in birds in general (Clifton et al., 2018; Raikow, 1970; Schreiweis, 1982; Setty, 1959), we observed that in the more terrestrial forms, the most distal point of the crista trochanteris is shifted somewhat more distally (Figure 6o–s). It is difficult to interpret this functionally, but it is possible that although these muscles play an important hip-stabilizing role in both FP and WP types (Clifton et al., 2018; Gatesy, 1999), this morphology of the crest itself may represent some advantage for the more terrestrial taxa.

The morphology of the proximal articulation differentiates some of the most advanced foot-propelled species—but interestingly to some extent the non-foot-propelled *Pelecanoides* specimens too—from the terrestrially more mobile taxa. The latter share features that possibly allows more mobility, with more degrees of flexion-extension and abduction-adduction in the hip joint (Figure 6o–s). In the case of *P. cristatus* and *P. carbo*, the proximal articulation is probably somewhat less mobile (Figure 6j–n): a femur with this possibly reduced mobility has a wide splay angle in an abducted position (Hertel & Campbell, 2007), which places the knees more laterally (while the tibiotarsus is positioned parasagittally), and thus the paddling is more lateral (Clifton et al., 2018). In their case, the facies articularis antitrochanterica also contacts the antitrochanter on a larger area, which thus supports the femur caudally, when the femoral splay angle is large. In terrestrially more mobile specimens, the trochlea fibularis on the distal epiphysis is narrow (Figure 6o–s), while in less terrestrial birds the robust condylus lateralis holds a broad trochlea fibularis—meaning a large fibular condyle angle, (see Hertel & Campbell, 2007)—which probably suggests a larger fibular head and well-developed fibula (Shufeldt, 1915) (Figure 6j–n).

What distinguishes the cormorant-type FP limb from the grebe-type, is the angle of the femoral neck (Figure 7b–g). As a result, the cormorant femur can adopt a more flexed position, which is less abducted, and therefore the knees are positioned more cranially than in grebes. This might explain why they retain some ability to move on land, while grebes are rather clumsy. The oblique morphology of the femoral neck of cormorants is most similar to that of ducks in our sample (Figure 7a), and maybe it increases the splay angle even when the femur is in a more flexed position. In contrast, the femora of the grebe are more abducted (and less flexed), and therefore their simultaneous synchronous limb strokes are more laterally directed (Johansson & Norberg, 2001), whereas in the cormorant the strokes are more ventrally directed (Johansson & Norberg, 2003; Schmid et al., 1995). Of the distal condyles, the medial one of cormorants (similar to the anatids'—Figure 7a) is more developed, and positioned somewhat more proximally; in contrast, grebes show a more developed condylus lateralis, which is approximately at the same level as the medial one. This condyle arrangement of cormorants and ducks might be related to their swimming/diving posture: due to the somewhat medially rotated knee, when the tibiotarsus is flexed it has a rather parasagittal position, and the ankle is placed more laterally (Owre, 1967; Provini et al., 2012).

In general, more terrestrial species show more robust tibiotarsus (Figure 8) and they also have a larger body mass (Figure S1g) (which is partly connected to the allometry—see below). It is noteworthy that *F. arctica*, known for its ambulatory adaptation among alcids (Johnsgard, 1987; Storer, 1945), shows a separation from its family towards the more robust tibiotarsi (Figure 8a). The proximocranial orientation of the cnemial crest present in these more terrestrial taxa (Figure 8b–e) could possibly be related to the articulation of the larger distal condyles of a robust femur, but could also be related to the patellae, and may indicate their large size. Although the role of the patella is not yet fully understood for all bird taxa, for some species it is known that it acts as a gear and can exert greater knee extension force (Allen et al., 2017), but it can also serve as an important muscle attachment site (Clifton et al., 2018). Cormorants and penguins are known to have large ('bulky') free patellae, which distally contact the proximal border of the cnemial crest (Setty, 1959; Shufeldt, 1883, 1884, 1913). These large knee structures could provide larger attachment sites for some of the hip stabilizer and knee extensor/stabilizer, ankle plantarflexor, and digital flexor muscles, that provide support for extensive paddling and/or rowing (Clifton et al., 2018). Nevertheless, Mayr et al. (2021) previously suggested, that the large patellae of penguins and cormorants might also be connected to their terrestrial upright posture. Because of the complex role of the patella, it is possible that this larger ('bulky'-type) patella could actually play a major role in both foot-propulsion and/or terrestrial locomotion in different taxa, especially as stable hip and knee and strong ankle plantarflexion might be beneficial not only in rowing but also in walking and stance. The strongly proximally elongated cnemial crest—characteristic of *P. cristatus* (Figure 8n–q)—

provides support for muscle attachments similar to the large patellae of cormorants. Species with lower cnemial crests may therefore either have other ways of increasing muscle attachment sites (such as the large free patella of cormorants) or they may not have a particularly developed foot-propelled locomotion form, or they may have a weaker hindlimb. The latter may be true, for example, for the dabbling duck *A. penelope*, or the alcids (Figure 8j–m). It is worth mentioning that, compared to the alcids', the cnemial crest of the *Pelecanoides* specimens is much more elongated proximally, although they use a similar (predominantly wing-based) aquatic locomotor type (Ryan & Nel, 1999).

The distal placement of the crista fibularis (Figure 8n–q) has been mentioned previously by Shufeldt (1883) for cormorants, and in some foot-propelled species (Anatidae, cormorants) we can also observe a widening of the crest (Figure 9f–i). This is difficult to interpret functionally, but the crest itself may have a strengthening role for the bone. Nevertheless, this feature coincides with the broad trochlea fibularis of the femur (Figure 6j–n), that is the large fibular head with developed fibulae (which is also true for grebes and for cormorants and *Pelecanoides* to a lesser extent), and may be related to the (knee flexor and hip extensor) muscles that attach to the fibula (Clifton et al., 2018), and which are important for leg propulsion.

A further specialization characteristic of cormorants and ducks is the way in which the medial condyle of the tibiotarsus extends cranially, increasing the angle of dorsiflexion of the tarsometatarsus, which might facilitate paddling movements, as was suggested by Zelenkov (2020). Furthermore, the medial orientation of the distal part of the tibiotarsus may also optimize the position of the intertarsal joint during foot propulsion, but may also help to step more medially during upright walking to support the center of mass (Provini, Simonis, & Abourachid, 2012). Although they are all foot-propelled divers or advanced surface paddlers, cormorants and ducks have a markedly different cnemial crest structure from that of grebes. Although in grebes the crista cnemialis cranialis and lateralis are less extended cranially and laterally, and they converge in the proximal direction, in anatids and cormorants they are overhanging cranially and laterally (Figure 9). This solution, complemented for example with large patellae, may increase the muscle attachment surfaces to some extent without elongating the crest in an extreme way.

4.3 | Allometry

When considering phylogeny, the effect of size on the shape of bones is not significant, except for the ulna. However, certain patterns are noteworthy. For the humerus and radius we were unable to explore the allometric signal for the overall shape data, but when looking at certain axes, it is clear that for all wing bones size-linked changes distinguish the non-wing-propelled taxa from the wing-propelled ones.

For the ulna, the increase in bone size is associated with the reduction of the epiphyses' size: the smallest ulnae belong to the wing-propelled volant *Pelecanoides* and *A. alle* (smallest and lightest birds in our dataset: Table S1), and thus associated with more robust epiphyses and larger cotyla ventralis, that might provide more stability through the proportionally larger joint surfaces and muscle attachment sites during the underwater actions of the wings (Supplementary I: Figure S4).

Larger size in hindlimb bones mostly corresponds with the increase in body mass (Supplementary I: Figures S5 and S6). The largest bones belong most of all to flightless species (Spheniscidae and *T. pteneres*), with good terrestrial capabilities. In contrast, the smallest species in our sample—the wing-propelled *Pelecanoides* and *A. alle*—are less mobile on land. However, our sightings might be biased since our sample does not include large birds (comparable to larger ducks or smaller penguins) that are clumsy on land, or mobile species similar in size to *Pelecanoides* and *A. alle*. Expansion of joint surfaces appears along with larger bone size in different ways: it is mediolateral for the proximal epiphysis of the femur and caudocranial for the proximal and distal epiphysis of the tibiotarsus. The mediolateral expansion of the proximal epiphysis, present on the larger femora possibly provides a more stable connection in the hip joint, and could also indicate more resistance to the constraints associated with holding or moving a larger body. Clumsy on land, *P. cristatus* is an exception in this respect, as it is characterized by higher allometric component values and a more mediolaterally elongated proximal epiphysis than species of similar size, which might be more related to leg stabilization in connection with its advanced foot-propelled abilities. The larger epiphyses on the large tibiotarsi might provide stability and a functional advantage in supporting a larger, heavier body, especially as the tibiotarsus in the bird's leg is the pillar-like element that provides static support (Abourachid & Höfling, 2012). This is consistent with *A. torda*, *Uria aalge*, and *P. cristatus* (clumsy on land) showing much less extensive epiphyses for their size (Figure S6).

5 | CONCLUSIONS

Aquatic birds encompass multiple locomotion types, as they show both aquatic, terrestrial, and even aerial skills. In this work, we attempted to quantitatively analyze the morphological variety of their limb bones in light of

locomotor abilities. The morphological traits outlined largely overlap with the phylogenetic relations, as we observed that phylogenetic heritage has a significant impact on morphology in all studied bones. Nevertheless, phylogeny has also a strong impact on bone size and locomotor abilities in our sample. The shape of the ulna, however, is proved to be influenced by size and aquatic propulsive techniques even when phylogeny is taken into account: enlarged epiphyses are present in wing-propelled taxa, which might contribute to increasing the stability of the wings, while species that do not use wing-propulsion are characterized by gracile epiphyses. Changes in the orientation of the cotyla ventralis of the ulna can also be linked to elbow stability: the flat joint surface of penguins decreases mobility, while the ulna morphology of the *Pelecanoides* specimens might contribute a better articulation to the humerus while remaining mobile. Besides, particular trends can be observed in those bones where the quantitative analyses resulted that the variation is primarily driven by phylogeny, which patterns might be related to ecologies and could be interpreted functionally as well. Separation of wing bones of taxa best adapted to wing-propulsion is generally linked to allometry. For the hindlimb bones, larger size relates to enlarged epiphyses, which is associated with better terrestrial capabilities. However, the robustness of the femur can also be related to foot-propulsion. In both volant and flightless wing-propelled species, the regions of origin of the triceps are larger on the humerus, which may indicate its important role in aquatic movements. In accordance with previous studies, the wing bones of the flightless wing-propelled penguins strongly differ from all other groups, as the wings have been modified into a rigid, flipper-like, structure used only for aquatic locomotion. Although for more terrestrial species the proximal articulation of the femur is mobile, the most foot-propelled taxa separate from them as they exhibit a femur morphology that reduces the proximal joint mobility but supports leg stability during swimming. Our analysis stressed the importance of different structures in the knee (e.g., enlarged cnemial crests) that can be linked to large muscle attachment sites, which might be beneficial not just for aquatic but for terrestrial movements for some species. Certain morphological similarities highlighted in the hindlimb bones of cormorants and ducks (foot-propelled taxa, that retained terrestrial abilities) might represent solutions to adopt leg postures suitable for both walking and swimming (oblique femoral neck, medially rotated knees, and medially bent distal tibiotarsus). Our preliminary analyses intended to enlighten phylogenetic, size, and functional signals in the stylopod and zeugopod bone morphology of aquatic birds. Further analyses on additional taxa and/or the use of curve and surface sliding semi-landmarks to better describe changes in the shape of the diaphysis, and/or additional bones, notably more distal bones (especially the tarsometatarsus) might enable a better discrimination between these different drivers of shape evolution.

AUTHOR CONTRIBUTIONS

Martin Segesdi: Data curation; methodology; writing – original draft; visualization; investigation; funding acquisition; project administration; conceptualization; formal analysis. **Delphine Brabant:** Data curation. **Raphaël Cornette:** Software; writing – review and editing; methodology. **Alexandra Houssaye:** Conceptualization; methodology; writing – review and editing; supervision; resources; project administration.

ACKNOWLEDGMENTS

We would like to thank Christine Lefèvre for providing access to the specimens for the analysis from the bird osteological collection of the MNHN (Paris). We are very grateful to Arnaud Delapré for his help during digitization. We are also grateful to Pauline Hanot, Camille Bader, Rémi Lefebvre, Cyril Etienne, Romain Pintore, Christophe Mallet, Idriss Pelletan, Romain Cottereau, Killian Leblanc, and Edina Prondvai for their help, advice, and for the helpful discussions. In addition, thanks are due to Attila Ősi, József Pálfy, and Miklós Kázmér for their scientific and administrative support. We also thank the anonymous reviewers for their comments on an earlier version of the manuscript, which contributed to improving the paper. We thank the three anonymous reviewers for their constructive and critical comments that improved our manuscript and the editor for her editorial work. Among the authors, MS dedicates this paper to the memory of the late József Szabó (1950–2023) who inspired him, and introduced him to the amazing world of Lake Velence, and from whom he first heard the phrase "*megy mint a vöcsök—goes like the grebe*." The Project was supported by the Erasmus+ programme and Tempus Public Foundation (Segesdi M.—CM-SMP-KA103/295472/2018 and 2021-1-HU01-KA131-HED-000003804).

CONFLICT OF INTEREST STATEMENT

The authors declare no conflict of interest.

DATA AVAILABILITY STATEMENT

The data that supports the findings of this study are available in the supplementary material of this article.

ORCID

Martin Segesdi https://orcid.org/0000-0003-4942-1810

REFERENCES

Abourachid, A., & Höfling, E. (2012). The legs: A key to bird evolutionary success. *Journal of Ornithology*, *153*, 193–198. https://doi.org/10.1007/s10336-012-0856-9

Adams, D. C. (2014). A generalized K statistic for estimating phylogenetic signal from shape and other high-dimensional multivariate data. *Systematic Biology*, *63*(5), 685–697. https://doi.org/10.1093/sysbio/syu030

Ainley, D. G. (1980). Birds as marine organisms: A review. *CalCOFI Reports*, *21*, 48–52.

Allen, V. R., Kambic, R. E., Gatesy, S. M., & Hutchinson, J. R. (2017). Gearing effects of the patella (knee extensor muscle sesamoid) of the helmeted guineafowl during terrestrial locomotion. *Journal of Zoology*, *303*, 178–187. https://doi.org/10.1111/jzo.12485

Ashmole, N. P. (1971). Seabird ecology and the marine environment. In D. S. Farner, J. S. King, & K. C. Parkes (Eds.), *Avian biology* (pp. 224–286). Academic Press.

Bader, C., Mallet, C., Chahoud, J., Amane, A., de Cupere, B., Berthon, R., Lavenne, F., Mohaseb, A., Davoudi, H., Albesso, M., Fathi, H., Vuillien, M., Lesur, J., Helmer, D., Gourichon, L., Hanotte, O., Mashkour, M., Vila, E., & Cucchi, T. (2022). Are petrous bones just a repository of ancient biomolecules? Investigating biosystematic signals in sheep petrous bones using 3D geometric morphometrics. *Journal of Archaeological Science: Reports*, *43*, 103447. https://doi.org/10.1016/j.jasrep.2022.103447

Baumel, J. J., King, A. S., Breazile, J. E., Evans, H. E., & Vanden Berge, J. C. (Eds.). (1993). *Handbook of avian anatomy: Nomina Anatomica Avium* (2nd ed.). Publications of Nuttall Ornithological Club.

Baumgart, S. L., Sereno, P. C., & Westneat, M. W. (2021). Wing shape in waterbirds: Morphometric patterns associated with behavior, habitat, migration, and phylogenetic convergence. *Integrative Organismal Biology (Oxford, England)*, *3*(1), obab011. https://doi.org/10.1093/iob/obab011

Baylac, M., & Frieß, M. (2005). Fourier descriptors, procrustes superimposition, and data dimensionality: An example of cranial shape analysis in modern human populations. In *Modern morphometrics in physical anthropology* (pp. 145–165). Springer US.

Bell, A., Marugán-Lobón, J., Navalón, G., Nebreda, S. M., DiGuildo, J., & Chiappe, L. M. (2021). Quantitative analysis of morphometric data of pre-modern birds: Phylogenetic versus ecological signal. *Frontiers in Earth Science*, *9*, 663342. https://doi.org/10.3389/feart.2021.663342

Bertelli, S., & Giannini, N. P. (2005). A phylogeny of extant penguins (Aves: Sphenisciformes) combining morphology and mitochondrial sequences. *Cladistics*, *21*(3), 209–239. https://doi.org/10.1111/j.1096-0031.2005.00065.x

Bjarnason, A., & Benson, R. (2021). A 3D geometric morphometric dataset quantifying skeletal variation in birds. *MorphoMuseuM*, *7*(1), e125. https://doi.org/10.18563/journal.m3.125

Blomberg, S. P., Garland, T., & Ives, A. R. (2003). Testing for phylogenetic signal in comparative data: Behavioral traits are more labile. *Evolution*, *57*(4), 717–745. https://doi.org/10.1111/j.0014-3820.2003.tb00285.x

Böhmer, C., Plateau, O., Cornette, R., & Abourachid, A. (2019). Correlated evolution of neck length and leg length in birds. *Royal Society Open Science*, *6*, 181588. https://doi.org/10.1098/rsos.181588

Bookstein, F. L. (1991). *Morphometric tools for landmark data: Geometry and biology*. Cambridge University Press.

Cignoni, P., Callieri, M., Corsini, M., Dellepiane, M., Ganovelli, F., & Ranzuglia, G. (2008). Meshlab: An open-source mesh processing tool. In *Eurographics Italian Chapter Conference* (Vol. 2008, pp. 129–136), The Eurographics Association. https://doi.org/10.2312/LocalChapterEvents/ItalChap/ItalianChapConf2008/129-136

Clark, G. A., Jr. (1993). Termini situm et directionem partium corporis indicantes. In *Handbook of avian anatomy: Nomina Anatomica Avium* (2nd ed.). Publications of Nuttall Ornithological Club.

Clifton, G. T., Carr, J. A., & Biewener, A. A. (2018). Comparative hindlimb myology of foot-propelled swimming birds. *Journal of Anatomy*, *232*(1), 105–123. https://doi.org/10.1111/joa.12710

De Blois, M. C., & Motani, R. (2019). Flipper bone distribution reveals flexible trailing edge in underwater flying marine tetrapods. *Journal of Morphology*, *280*, 908–924. https://doi.org/10.1002/jmor.20992

De Mendoza, R. S., & Gómez, R. O. (2022). Ecomorphology of the tarsometatarsus of waterfowl (Anseriformes) based on geometric morphometrics and its application to fossils. *The Anatomical Record*, *305*(11), 3243–3253. https://doi.org/10.1002/ar.24891

Dunning, J. B., Jr. (2008). *CRC handbook of avian body masses* (2nd ed.). CRC Press. https://doi.org/10.1201/9781420064452

Ericson, P. G. P., Anderson, C. L., Britton, T., Elzanowski, A., Johansson, U. S., Källersjö, M., Ohlson, J. I., Parsons, T. J., Zuccon, D., & Mayr, G. (2006). Diversification of Neoaves: Integration of molecular sequence data and fossils. *Biology Letters*, *2*, 543–547. https://doi.org/10.1098/rsbl.2006.0523

Felice, R. N., & Goswami, A. (2018). Developmental origins of mosaic evolution in the avian cranium. *Proceedings of the National Academy of Sciences of the United States of America*, *115*(3), 555–560. https://doi.org/10.1073/pnas.1716437115

Fish, F. E. (2016). Secondary evolution of aquatic propulsion in higher vertebrates: Validation and prospect. *Integrative and Comparative Biology*, *56*(6), 1285–1297. https://doi.org/10.1093/icb/icw123

Friesen, V. L., Baker, A. J., & Piatt, J. F. (1996). Phylogenetic relationships within the Alcidae (Charadriiformes: Aves) inferred from total molecular evidence. *Molecular Biology and Evolution*, *13*(2), 359–367. https://doi.org/10.1093/oxfordjournals.molbev.a025595

Fritz, S. A., & Purvis, A. (2010). Selectivity in mammalian extinction risk and threat types: A new measure of phylogenetic signal strength in binary traits. *Conservation Biology*, *24*(4), 1042–1051.

Fulton, T. L., Letts, B., & Shapiro, B. (2012). Multiple losses of flight and recent speciation in steamer ducks. *Proceedings of the Royal Society B: Biological Sciences*, *279*(1737), 2339–2346. https://doi.org/10.1098/rspb.2011.2599

Gatesy, S. M. (1999). Guineafowl hind limb function. II: Electromyographic analysis and motor pattern evolution. *Journal of Morphology*, *240*, 127–142. https://doi.org/10.1002/(SICI)1097-4687(199905)240:2<127::AID-JMOR4>3.0.CO;2-Q

Gonzalez, J., Düttmann, H., & Wink, M. (2009). Phylogenetic relationships based on two mitochondrial genes and hybridization

patterns in Anatidae. *Journal of Zoology*, *279*(3), 310–318. https://doi.org/10.1111/j.1469-7998.2009.00622.x

Gower, J. C. (1975). Generalized procrustes analysis. *Psychometrika*, *40*(1), 33–51. https://doi.org/10.1007/BF02291478

Gunz, P., & Mitteroecker, P. (2013). Semilandmarks: A method for quantifying curves and surfaces. *Hystrix, The Italian. Journal of Mammalogy*, *24*(1), 103–109. https://doi.org/10.4404/hystrix-24.1-6292

Gunz, P., Mitteroecker, P., Neubauer, S., Weber, G. W., & Bookstein, F. L. (2009). Principles for the virtual reconstruction of hominin crania. *Journal of Human Evolution*, *57*(1), 48–62. https://doi.org/10.1016/j.jhevol.2009.04.004

Gutarra, S., & Rahman, I. A. (2022). The locomotion of extinct secondarily aquatic tetrapods. *Biological Reviews*, *97*(1), 67–98. https://doi.org/10.1111/brv.12790

Hackett, S. J., Kimball, R. T., Reddy, S., Bowie, R. C. K., Braun, E. L., Braun, M. J., Chojnowski, J. L., Cox, W. A., Han, K. L., Harshman, J., Huddleston, C. J., Marks, B. D., Miglia, K. J., Moore, W. S., Sheldon, F. H., Steadman, D. W., Witt, C. C., & Yuri, T. (2008). A phylogenomic study of birds reveals their evolutionary history. *Science*, *320*(5884), 1763–1768. https://doi.org/10.1126/science.1157704

Haidr, N. S., & Hospitaleche, C. A. (2017). New data on the humeral triceps of penguins and its implications in the evolution of the fossa tricipitalis. *Historical Biology*, *31*(7), 853–856. https://doi.org/10.1080/08912963.2017.1396324

Hertel, F., & Campbell, K. E. (2007). The antitrochanter of birds: Form and function in balance (El Antitrocánter en las Aves: Forma y Función en el Equilibrio). *The Auk*, *124*(3), 789–805.

Hinić-Frlog, S., & Motani, R. (2010). Relationship between osteology and aquatic locomotion in birds: Determining modes of locomotion in extinct Ornithurae. *Journal of Evolutionary Biology*, *23*(2), 372–385. https://doi.org/10.1111/j.1420-9101.2009.01909.x

Houssaye, A. (2009). "Pachyostosis" in aquatic amniotes: A review. *Integrative Zoology*, *4*(4), 325–340. https://doi.org/10.1111/j.1749-4877.2009.00146.x

Houssaye, A., & Fish, F. E. (2016). Functional (secondary) adaptation to an aquatic life in vertebrates: An introduction to the symposium. *Integrative and Comparative Biology*, *56*(6), 1266–1270. https://doi.org/10.1093/icb/icw129

Hui, C. A. (1988). Penguin swimming II. Energetics and behavior. *Physiological Zoology*, *61*(4), 344–350.

Hustler, K. (1992). Buoyancy and its constraints on the underwater foraging behaviour of Reed Cormorants *Phalacrocorax africanus* and Darters *Anhinga melanogaster*. *Ibis*, *134*(3), 229–236. https://doi.org/10.1111/j.1474-919X.1992.tb03804.x

Jarvis, E. D., Mirarab, S., Aberer, A. J., Li, B., Houde, P., Li, C., Ho, S. Y. W., Faircloth, B. C., Nabholz, B., Howard, J. T., Suh, A., Weber, C. C., da Fonseca, R. R., Li, J., Zhang, F., Li, H., Zhou, L., Narula, N., Liu, L., ... Zhang, G. (2014). Whole-genome analyses resolve early branches in the tree of life of modern birds. *Science*, *346*(6215), 1320–1331. https://doi.org/10.1126/science.1253451

Jenkins, F. A., Jr. (1993). The evolution of the avian shoulder joint. *American Journal of Science*, *293*, 253–267. https://doi.org/10.2475/ajs.293.a.253

Jetz, W., Thomas, G. H., Joy, J. B., Hartmann, K., & Mooers, A. O. (2012). The global diversity of birds in space and time. *Nature*, *491*, 444–448. https://doi.org/10.1038/nature11631

Johansson, L. C., & Norberg, R. Å. (2003). Delta-wing function of webbed feet gives hydrodynamic lift for swimming propulsion in birds. *Nature*, *424*, 65–68. https://doi.org/10.1038/nature01695

Johansson, L. C., & Norberg, U. M. L. (2001). Lift-based paddling in diving grebe. *Journal of Experimental Biology*, *204*(10), 1687–1696. https://doi.org/10.1242/jeb.204.10.1687

Johnsgard, P. A. (1987). *Diving birds of North America [complete book]*. University of Nebraska Press, University of Nebraska–Lincoln Libraries. [ebook edition].

Kelley, N. P., & Pyenson, N. D. (2015). Evolutionary innovation and ecology in marine tetrapods from the Triassic to the Anthropocene. *Science*, *348*(6232), aaa3716. https://doi.org/10.1126/science.aaa3716

Klingenberg, C. P. (2016). Size, shape, and form: Concepts of allometry in geometric morphometrics. *Development Genes and Evolution*, *226*(3), 113–137. https://doi.org/10.1007/s00427-016-0539-2

Kooyman, G. L. (1989). *Diverse divers*. Springer Verlag.

Krahl, A., & Werneburg, I. (2022). Deep-time invention and hydrodynamic convergences through amniote flipper evolution. *The Anatomical Record*, *306*(6), 1323–1355. https://doi.org/10.1002/ar.25119

Ksepka, D. T., & Ando, T. (2011). Penguins past, present, and future: Trends in the evolution of the Sphenisciformes. In G. Dyke & G. Kaiser (Eds.), *Living dinosaurs: The evolutionary history of modern birds* (pp. 155–186). John Wiley & Sons. https://doi.org/10.1002/9781119990475.ch6

Lapsansky, A. B., & Armstrong, R. H. (2022). Common mergansers *Mergus merganser* use wings to pursue a fish underwater. *Marine Ornithology*, *50*, 111–114.

Lapsansky, A. B., Warrick, D. R., & Tobalske, B. W. (2022). High wing-loading correlates with dive performance in birds, suggesting a strategy to reduce buoyancy. *Integrative and Comparative Biology*, *62*(4), 878–889. https://doi.org/10.1093/icb/icac117

Livezey, B. C. (1986). Phylogeny and historical biogeography of steamer-ducks (Anatidae: Tachyeres). *Systematic Zoology*, *35*(4), 458–469. https://doi.org/10.2307/2413109

Louw, G. J. (1992). Functional anatomy of the penguin flipper. *Journal of the South African Veterinary Association*, *63*(3), 113–120.

Lovvorn, J., Liggins, G. A., Borstad, M. H., Calisal, S. M., & Mikkelsen, J. (2001). Hydrodynamic drag of diving birds: Effects of body size, body shape and feathers at steady speeds. *The Journal of Experimental Biology*, *204*(Pt 9), 1547–1557. https://doi.org/10.1242/jeb.204.9.1547

Maddison, W. P., & Maddison, D. R. (2021). Mesquite: A modular system for evolutionary analysis. Version 3.81, Available from: http://www.mesquiteproject.org.

Mayr, G., Goedert, J. L., de Pietri, V. L., & Scofield, R. P. (2021). Comparative osteology of the penguin-like mid-Cenozoic Plotopteridae and the earliest true fossil penguins, with comments on the origins of wing-propelled diving. *Journal of Zoological Systematics and Evolutionary Research*, *59*, 264–276. https://doi.org/10.1111/jzs.12400

McKitrick, M. C. (1991). Forelimb myology of loons (Gaviiformes), with comments on the relationship of loons and tubenoses (Procellariiformes). *Zoological Journal of the Linnean Society*, *102*, 115–152. https://doi.org/10.1111/j.1096-3642.1991.tb00285.x

Mitteroecker, P., & Gunz, P. (2009). Advances in geometric Morphometrics. *Evolutionary Biology*, *36*, 235–247. https://doi.org/10.1007/s11692-009-9055-x

Mitteroecker, P., Gunz, P., Bernhard, M., Schaefer, K., & Bookstein, F. L. (2004). Comparison of cranial ontogenetic trajectories among great apes and humans. *Journal of Human Evolution*, *46*, 679–698. https://doi.org/10.1016/j.jhevol.2004.03.006

Motani, R., & Vermeij, G. J. (2021). Ecophysiological steps of marine adaptation in extant and extinct non-avian tetrapods. *Biological Reviews*, *96*(5), 1769–1798. https://doi.org/10.1111/brv.12724

Moum, T., Arnason, U., & Árnason, E. (2002). Mitochondrial DNA sequence evolution and phylogeny of the Atlantic Alcidae, including the extinct great auk (*Pinguinus impennis*). *Molecular Biology and Evolution*, *19*(9), 1434–1439. https://doi.org/10.1093/oxfordjournals.molbev.a004206

Navalón, G., Bjarnason, A., Griffiths, E., & Benson, R. B. J. (2022). Environmental signal in the evolutionary diversification of bird skeletons. *Nature*, *611*(7935), 306–311. https://doi.org/10.1038/s41586-022-05372-y

Owre, O. T. (1967). Adaptations for locomotion and feeding in the anhinga and the double-crested cormorant. *Ornithological Monographs*, *6*, 1–138.

Paradis, E., Claude, J., & Strimmer, K. (2004). APE: Analyses of phylogenetics and evolution in R language. *Bioinformatics*, *20*, 289–290. https://doi.org/10.1093/bioinformatics/btg412

Provini, P., Goupil, P., Hugel, V., & Abourachid, A. (2012). Walking, paddling, waddling: 3D kinematics anatidae locomotion (*Callonetta leucophrys*). *Journal of Experimental Zoology*, *317*, 275–282. https://doi.org/10.1002/jez.1721

Provini, P., & Höfling, E. (2020). To hop or not to hop? The answer is in the bird trees. *Systematic Biology*, *69*(5), 962–972. https://doi.org/10.1093/sysbio/syaa015

Provini, P., Simonis, C., & Abourachid, A. (2012). Functional implications of the intertarsal joint shape in a terrestrial (*Coturnix coturnix*) versus a semi-aquatic bird (*Callonetta leucophrys*). *Journal of Zoology*, *290*, 12–18. https://doi.org/10.1111/jzo.12007

R Development Core Team. (2014). *R: A language and environment for statistical computing*. R Foundation for Statistical Computing. Available at http://www.R-project.org/.

Raikow, R. J. (1970). Evolution of diving adaptations in the stifftail ducks. *University of California Publications in Zoology.*, *94*, 1–52.

Raikow, R. J., Bicanovsky, L., & Bledsoe, A. H. (1988). Forelimb joint mobility and the evolution of wing-propelled diving in birds. *The Auk*, *105*(3), 446–451.

Revell, L. J. (2012). Phytools: An R package for phylogenetic comparative biology (and other things). *Methods in Ecology and Evolution*, *3*, 217–223. https://doi.org/10.1111/j.2041-210X.2011.00169.x

Ripley, B. D. (2007). *Pattern recognition and neural networks*. Cambridge University Press.

Rohlf, F. J., & Slice, D. (1990). Extensions of the procrustes method for the optimal superimposition of landmarks. *Systematic Biology*, *39*(1), 40–59. https://doi.org/10.2307/2992207

Rubolini, D., Liker, A., Garamszegi, L. Z., Møller, A. P., & Saino, N. (2015). Using the BirdTree.Org website to obtain robust phylogenies for avian comparative studies: A primer. *Current Zoology*, *61*(6), 959–965. https://doi.org/10.1093/czoolo/61.6.959

Ryan, P. G., & Nel, D. C. (1999). Foraging behaviour of diving petrels *Pelecanoides*. *Emu - Austral Ornithology*, *99*(1), 72–74. https://doi.org/10.1071/MU99009B

Schmid, D., Grémillet, D. J. H., & Culik, B. M. (1995). Energetics of underwater swimming in the great cormorant (*Phalacrocorax carbo sinensis*). *Marine Biology*, *123*, 875–881.

Schreiweis, D. O. (1982). *A comparative study of the appendicular musculature of penguins (Aves, Sphenisciformes)* (pp. 1–46). Smithsonian Institution Press. https://doi.org/10.5479/si.00810282.341

Segesdi, M., & Pecsics, T. (2022). Trends of avian locomotion in water – An overview of swimming styles. *Ornis Hungarica*, *30*(1), 30–46. https://doi.org/10.2478/orhu-2022-0003

Serrano, F. J., Costa-Pérez, M., Navalón, G., & Martín-Serra, A. (2020). Morphological disparity of the humerus in modern birds. *Diversity*, *12*(5), 173. https://doi.org/10.3390/d12050173

Setty, L. R. (1959). Muscles of the hip and thigh of the emperor penguin. *Journal of the Washington Academy of Sciences*, *49*(6), 183–187.

Shealer, D. A. (2002). Foraging behavior and food of seabirds. In E. A. Schreiber & J. Burger (Eds.), *Biology of marine birds* (pp. 137–177). CRC Press.

Shufeldt, R. W. (1883). Remarks upon the osteology of *Phalacrocorax bicristatus*. *Science*, *ns-2*, 640–642. https://doi.org/10.1126/science.ns-2.41.640

Shufeldt, R. W. (1884). Concerning some of the forms assumed by the patella in birds. *Proceedings of the United States National Museum.*, *7*(439), 324–331. https://doi.org/10.5479/si.00963801.7-439.324

Shufeldt, R. W. (1913). On the patella in the Phalacrocoracidae. *Proceedings of the Zoological Society of London*, *83*, 393–402.

Shufeldt, R. W. (1915). Comparative osteology of Harris's flightless cormorant (*Nannopterum harrisi*). *Emu*, *15*(2), 86–114.

Sidlauskas, B. (2008). Continuous and arrested morphological diversification in sister clades of characiform fishes: A phylomorphospace approach. *Evolution*, *62*, 3135–3156. https://doi.org/10.1111/j.1558-5646.2008.00519.x

Smith, N. A., Koeller, K. L., Clarke, J. A., Ksepka, D. T., Mitchell, J. S., Nabavizadeh, A., Ridgley, R. C., & Witmer, L. M. (2021). Convergent evolution in dippers (Aves, Cinclidae): The only wing-propelled diving songbirds. *The Anatomical Record*, *305*(7), 1563–1591. https://doi.org/10.1002/ar.24820

Storer, R. W. (1945). Structural modifications in the hind limb in the Alcidae. *Ibis*, *87*(3), 433–456. https://doi.org/10.1111/j.1474-919X.1945.tb01375.x

Townsend, C. W. (1909). The use of the wings and feet by diving birds. *The Auk*, *26*(3), 234–248.

Vazquez, R. J. (1994). The automating skeletal and muscular mechanisms of the avian wing (Aves). *Zoomorphology*, *114*, 59–71. https://doi.org/10.1007/BF00574915

Venables, W. N., & Ripley, B. D. (2002). In S. Fourth (Ed.), *Modern applied statistics*. Springer, York. Springer.

Wang, X., & Clarke, J. A. (2014). Phylogeny and forelimb disparity in waterbirds. *Evolution*, *68*, 2847–2860. https://doi.org/10.1111/evo.12486

Wang, X., & Clarke, J. A. (2015). The evolution of avian wing shape and previously unrecognized trends in covert feathering. *Proceedings. Biological Sciences*, *282*(1816), 20151935. https://doi.org/10.1098/rspb.2015.1935

Watanabe, J. (2018). Ontogeny of surface texture of limb bones in modern aquatic birds and applicability of textural ageing. *The Anatomical Record*, *301*(6), 1026–1045. https://doi.org/10.1002/ar.23736

Watanabe, J., Field, D. J., & Matsuoka, H. (2021). Wing musculature reconstruction in extinct flightless auks (*Pinguinus* and *Mancalla*) reveals incomplete convergence with penguins (Spheniscidae) due to differing ancestral states. *Integrative Organismal Biology*, *3*(1), obaa040. https://doi.org/10.1093/iob/obaa040

Wiley, D. F., Amenta, N., Alcantara, D., Ghosh, D., Kil, Y. J., Delson, E., Harcourt-Smith, W., Rohlf, F. J., St John, K., & Hamann, B. (2005). Evolutionary morphing. In *VIS 05. IEEE Visualization, 2005* (pp. 431–438). IEEE. https://doi.org/10.1109/VISUAL.2005.1532826

Zelenkov, N. (2020). The oldest diving anseriform bird from the late Eocene of Kazakhstan and the evolution of aquatic adaptations in the intertarsal joint of waterfowl. *Acta Palaeontologica Polonica*, *65*(4), 733–742. Available from:. https://doi.org/10.4202/app.00764.2020

SUPPORTING INFORMATION

Additional supporting information can be found online in the Supporting Information section at the end of this article.

How to cite this article: Segesdi, M., Brabant, D., Cornette, R., & Houssaye, A. (2024). How does the shape of the wing and hindlimb bones of aquatic birds relate to their locomotor abilities? *The Anatomical Record*, 1–29. https://doi.org/10.1002/ar.25512